Toxicology 454 (2021) 152737

Contents lists available at ScienceDirect

Toxicology

journal homepage: www.elsevier.com/locate/toxicol

Neurotoxic and convulsant effects induced by jack bean ureases on the mammalian nervous system

Carlos Gabriel Moreira Almeida [a,b], Kiyo Costa-Higuchi [a,c], Angela Regina Piovesan [a,d], Carlo Frederico Moro [a,b], Gianina Teribele Venturin [e], Samuel Greggio [e], Zaquer Susana Costa-Ferro [f], Simone Denise Salamoni [f], Steve Peigneur [g], Jan Tytgat [g], Maria Elena de Lima [h], Carolina Nunes da Silva [i], Lúcia Vinadé [j], Edward G. Rowan [k], Jaderson Costa DaCosta [f], Chárisston André Dal Belo [j,**], Celia Regina Carlini [a,b,l,*]

[a] Laboratory of Neurotoxins, Brain Institute of Rio Grande do Sul (BraIns), Pontifícia Universidade Católica do Rio Grande do Sul, Porto Alegre, RS, Brazil
[b] Graduate Program in Medicine and Health Sciences, School of Medicine, Pontifícia Universidade Católica do Rio Grande do Sul, Porto Alegre, RS, Brazil
[c] Graduate Program in Materials Technology and Engineering, Pontifícia Universidade Católica do Rio Grande do Sul, Porto Alegre, RS, Brazil
[d] Graduate Program in Celular and Molecular Biology, Center of Biotechnology, Universidade Federal do Rio Grande do Sul, Porto Alegre, Brazil
[e] Preclinical Research Center, Brain Institute of Rio Grande do Sul (BraIns), Pontifícia Universidade Católica do Rio Grande do Sul, Porto Alegre, RS, Brazil
[f] Laboratory of Neuroscience, Brain Institute of Rio Grande do Sul (BraIns), Pontifícia Universidade Católica do Rio Grande do Sul, Porto Alegre, RS, Brazil
[g] Laboratory of Toxicology & Pharmacology, University of Leuven (KU Leuven), Leuven, Belgium
[h] Institute of Teaching and Research, Santa Casa de Belo Horizonte, Belo Horizonte, MG, Brazil
[i] Faculty of Pharmacy, Universidade Federal de Minas Gerais, Belo Horizonte, MG, Brazil
[j] Laboratory of Neurobiology and Toxinology (Lanetox), Universidade Federal do Pampa, São Gabriel, RS, Brazil
[k] Strathclyde Institute for Biomedical Sciences, University of Strathclyde, Glasgow, UK
[l] Scholl of Medicine, Pontificía Universidade Católica do Rio Grande do Sul, Porto Alegre, RS, Brazil

ARTICLE INFO

Keywords:
Canatoxin
Epileptogenesis
Ion channels
Positron emission tomography
Long term potentiation
L-glutamate

ABSTRACT

Ureases are microbial virulence factors either because of the enzymatic release of ammonia or due to many other non-enzymatic effects. Here we studied two neurotoxic urease isoforms, Canatoxin (CNTX) and Jack Bean Urease (JBU), produced by the plant *Canavalia ensiformis*, whose mechanisms of action remain elusive. The neurotoxins provoke convulsions in rodents (LD_{50} ~2 mg/kg) and stimulate exocytosis in cell models, affecting intracellular calcium levels. Here, electrophysiological and brain imaging techniques were applied to elucidate their mode of action. While systemic administration of the toxins causes tonic-clonic seizures in rodents, JBU injected into rat hippocampus induced spike-wave discharges similar to absence-like seizures. JBU reduced the amplitude of compound action potential from mouse sciatic nerve in a tetrodotoxin-insensitive manner. Hippocampal slices from CNTX-injected animals or slices treated *in vitro* with JBU failed to induce long term potentiation upon tetanic stimulation. Rat cortical synaptosomes treated with JBU released L-glutamate. JBU increased the intracellular calcium levels and spontaneous firing rate in rat hippocampus neurons. MicroPET scans of CNTX-injected rats revealed increased $^{[18]}$Fluoro-deoxyglucose uptake in epileptogenesis-related areas like hippocampus and thalamus. Curiously, CNTX did not affect voltage-gated sodium, calcium or potassium channels currents, neither did it interfere on cholinergic receptors, suggesting an indirect mode of action that could be related to the ureases' membrane-disturbing properties. Understanding the neurotoxic mode of action of *C. ensiformis* ureases could help to unveil the so far underappreciated relevance of these toxins in diseases caused by urease-producing microorganisms, in which the human central nervous system is affected.

Abbreviations: CNTX, canatoxin; JBU, major jack bean urease; LTP, long term potentiation; microPET, positron emission microtomography.

* Corresponding author at: Laboratory of Neurotoxins, Brain Institute of Rio Grande do Sul (BraIns), Pontifícia Universidade Católica do Rio Grande do Sul, Porto Alegre, RS, CEP 90.610-000, Brazil.
** Corresponding author at: Laboratory of Neurobiology and Toxinology (Lanetox), Universidade Federal do Pampa, São Gabriel, RS, Brazil.
E-mail addresses: charistondb@unipampa.br (C.A. Dal Belo), celia.carlini@pucrs.br (C.R. Carlini).

https://doi.org/10.1016/j.tox.2021.152737
Received 9 November 2020; Received in revised form 18 January 2021; Accepted 20 February 2021
Available online 22 February 2021

1. Introduction

Ureases (urea amidohydrolases; EC 3.5.1.5), enzymes that catalyze the hydrolysis of urea into carbon dioxide and ammonia, are *moonlighting* proteins, a name to address proteins that have different non-associated biological activities (Jeffery, 1999). Ureases are toxins with a defense role and/or that act as virulence factors for the producing organisms both because of their enzymatic activity that forms the toxic compound ammonia, or due to their non-enzymatic biological activities. Regardless of the source, ureases share at least 55 % identity of their amino acids sequences and have similar 3D structures despite the differences in their quaternary organization (for a review, see Kappaun et al., 2018). However, despite their widespread presence in pathogenic microorganisms, conserved structures and enzymatic action, little is known about the contribution of ureases to mechanisms of diseases except that of enabling pathogen survival in acidic environments within their hosts.

In 1926, James B. Sumner isolated a urease from jack beans (*Canavalia ensiformis*), named as Jack bean urease (JBU), the first enzyme ever obtained in a crystalline form, demonstrating that enzymes could be proteins. The basic structural unity of JBU is a single polypeptide chain with 840 amino acid residues and a molecular mass of 90,770 Da (Riddles et al., 1991).

In 1981, a convulsant protein, designated as Canatoxin (CNTX), was isolated from *Canavalia ensiformis* seeds (Carlini and Guimaraes, 1981). Canatoxin was later characterized as an isoform of JBU, the latter more abundant in seeds (Follmer et al., 2001). Canatoxin induces seizures and death when injected *i.p.* in mice and rats, but it is inactive when given orally (Carlini and Guimaraes, 1981). JBU is also neurotoxic and lethal to mice (Follmer et al., 2001). *In vitro,* CNTX induces exocytosis in platelets, synaptosomes, pancreatic islets and mastocytes (Barja-Fidalgo et al., 1991a, b; Ghazaleh et al., 1997; Grassi-Kassisse and Ribeiro-DaSilva, 1992). These effects are mediated by eicosanoids and increased intracellular levels of calcium (Barja-Fidalgo et al., 1991b; Ghazaleh et al., 1997). CNTX inhibited the accumulation of calcium by rabbit inside-out sarcoplasmatic reticulum vesicles, uncoupling the ion transport by the Ca^{2+}-ATPase from its enzyme activity (Alves et al., 1992). CNTX promoted dopamine and serotonin secretion in rat brain synaptosomes to the same extent as that obtained with KCl depolarization (Barja-Fidalgo et al., 1991b). *In vivo,* CNTX produces bradycardia, hypothermia, hyperglycemia and hypotension in rats (Carlini et al., 1984), contrasting to a hypertension-inducing effect expected for convulsant drugs (Antonaccio and Taylor, 1977; Persson and Henning, 1980). More recently, studies have indicated that JBU is capable of inserting itself into lipid bilayers, altering physicochemical properties of artificial membranes, and forming cation-selective ion channels (Micheletto et al., 2016; Piovesan et al., 2014). These findings pointed to the complexity of the neurotoxic effects of CNTX and of its isoform, JBU. So far, the cellular site and the molecular target(s) of *C. ensiformis* ureases that trigger neurotoxicity are only partially understood.

In an attempt to unveil this mechanism of action, here electrophysiological and brain imaging techniques were applied to elucidate CNTX's and JBU's mode of action. The data collected on the mechanisms of neurotoxicity triggered by these plant ureases may help through light on the so far underappreciated role of microbial ureases as virulence factors, particularly in the case of pathogenic microorganisms causing illness with neurotoxic symptoms.

2. Methods

2.1. Reagents

All chemicals and reagents used were of the highest purity available and were purchased from Sigma-Aldrich, Merck or BioRad.

2.2. C. ensiformis ureases

Canatoxin and jack bean urease were isolated from *Canavalia ensiformis* seeds (Casa Agrodora, São Paulo, Brazil) and purified as previously described (Follmer et al., 2001, 2004b; Weber et al., 2008). Molecular masses of 540 kDa for JBU and of 185 kDa for CNTX (Follmer et al., 2001) were considered for determining molar concentrations. CNTX was used in all protocols requiring intraperitoneal administration. For the other protocols, CNTX and/or JBU were used according to availability. Depending on the type of experimental protocol, doses (0.2 mg–2.0 mg kg animal body weight) or concentrations (1 nM up to 1 μM) of ureases were chosen in accordance to previous published data with CNTX or JBU.

Although the amount of urease released *in vivo* in humans infected by urease-producing pathogenic microorganism is not known, the levels of JBU/CNTX employed in the experiments were low enough (nanomolar range) to eventually match those of microbial ureases acting as virulence factors in many pathologies. Ureases can reach the CNS from peripheral sites of infection through a weakened blood brain barrier caused by hyperammonemia and/or low grade chronic inflammation or transported inside outer membrane vesicles released by urease-producing microorganisms (Jan, 2017; Skowronska and Albrecht, 2012).

2.3. Animals

Male adult Swiss mice (28–35 g) and female Wistar rats (150–200 g) were obtained from the Center for Biological Experimental Models (CeMBE), from the Pontifical Catholic University of Rio Grande do Sul (PUCRS), Porto Alegre, RS, Brazil. The animals were housed at 25 °C with access *ad libitum* to food and water and 12 h light-dark cycles. All animal protocols in this work were done in accordance with the ARRIVE guidelines and the National Institutes of Health guide for Laboratory animals (NIH Publications No. 8023, revised 1978), and approved by the local animal care committee, under the authorization number 7907/2018 (PUCRS-CEUA).

Xenopus laevis female frogs were obtained from the Centre de Ressources Biologiques Xénopes, France. The use of frogs was in accordance with the license number LA1210239 of the Laboratory of Toxicology & Pharmacology, University of Leuven, Belgium. All animal care and experimental procedures agreed with the guidelines of the "European convention for the protection of vertebrate animals used for experimental and other scientific purposes" (Strasbourg, 18.III.1986).

2.4. Electrode implantation for electroencephalographic recordings

Animals were anesthetized with ketamine (90 $mg.kg^{-1}$) and xylazine (13 $mg.kg^{-1}$). The anesthesia was maintained with extra doses of ketamine/xylazine (30 % of initial dose), after checking the tail pinch reflex and respiratory rate. Body temperature was maintained at 37 ± 0.5 °C using a heating pad. For the EEG recordings, A-M SYSTEMS .0045" tungsten Teflon-insulated electrodes were employed. These electrodes were surgically implanted on mPFC (3.0 mm anterior to bregma, 0.4 mm lateral to midline and 3.2 mm ventral to dura mater); CA_1 (5.7 mm anterior to bregma, 4.6 mm lateral to midline and 2.5 mm ventral to dura mater) and TMD (-1.9 mm anterior to bregma, -0.4 mm to midline and -4.8 mm ventral to dura mater). The electrode implanting sites coordinates followed Paxinos and Watson (2007). A chemitrode (electrode plus cannula) was implanted on the hippocampal CA_1 area. The cannula was used for intrahippocampal injections of JBU (0.018 μg. kg^{-1} body weight) in a volume of 2 μL. The skull was exposed, and holes were drilled so that the recording electrodes and the chemitrode could be lowered at the mentioned stereotaxic coordinates. An additional hole was drilled over the parietal to cortex to implant a micro screw that served as a recording reference (ground). An additional electrode was used as electromyogram to record the electrical activity of the animal's neck muscles and detect REM sleep, noise caused by body movements or

electrical oscillations.

2.5. Rat electroencephalographic (EEG) recordings

EEG was recorded by an electroencephalograph (NIHONCOHDEN, Japan, Tokyo) attached to a device for data capture and analysis (CED: Cambridge Electronic Design Ltd., UK, Cambridge; POWER 1401 mkII). Sampling rate was 2,000 Hz whereas the bandwidth of the EEG recording was 0.3–150 Hz. The number of SWDs (spike and wave discharge; frequency between 3–11 Hz; a train of asymmetric spikes and slow waves starting and ending with sharp spikes; the average amplitude at least twice as high as the basal EEG activity) (Kovacs et al., 2015) and time of SWDs (average time and total time of SWDs) were measured between 30 and 270 min of post-injection time (from 4.00 PM to 8.00 PM). The software used to acquire the data was LabChart 7 from ADinstruments Inc., 2205 Colorado Springs CO 80906, USA.

EEG recordings were carried out in awake rats without anesthesia during 6 h, in a recording chamber containing food and water *ad libitum*. After 2 h of basal recordings, the animals were injected with JBU 0.018 $\mu g.kg^{-1}$ by using a Hamilton syringe connected to a 30 G dental needle, through a flexible polypropylene pipe. The needle was inserted into the cannula and stood 0.1 mm above hippocampal CA_1. The total volume of the JBU (2 µL) solution was injected in one minute.

2.6. Primary culture of rat hippocampus cells

Primary hippocampal cultures were prepared as described previously (Domingues et al., 2018). Briefly, 1- to 2-day-old Wistar rats were killed by cervical dislocation and decapitated. Once the hippocampi were removed and triturated, cells were plated at a density of 0.5×10^{56} cells. mL^{-1} onto poly-L-lysine coated covers lips. Cultures were incubated in a medium consisting of Neurobasal-A Medium (Invitrogen, Paisley, UK) supplemented with 2% (v/v) B-27 (Invitrogen) and 2 mM L-glutamine and maintained in a humidified atmosphere at 37 °C, 5% CO_2 for 10–14 days in vitro (DIV). All experiments were performed on cells taken from at least three separate cultures obtained from different rats.

2.7. Ca^{2+} imaging of primary hippocampal cultures

Ca^{2+} imaging experiments were performed following the method described in Domingues et al. (2018). All imaging experiments were performed on a digital epifluorescence imaging system (WinFluor, J. Dempster, University of Strathclyde) mounted on a Nikon TE 2000 microscope using a 20x objective. Hippocampal cultures (DIV 10–14) were loaded with FLUO-4 AM (5 µM, 45–60 min, room temperature, Invitrogen) prior to experiments. Experiments were performed on cultures continually perfused (1–2 $mL.min^{-1}$) with HEPES-buffered saline containing (in mM): NaCl 140, KCl 5, $MgCl_2$ 2, $CaCl_2$ 2, HEPES 10, D-glucose 10, pH 7.4 and osmolarity adjusted to 310 mOsm with sucrose, if required. Drugs were added via the perfusate. Ratiometric images (340/380 nm) were obtained from the somata of cells every 300 ms during 10 min. Cells were identified as astrocytes based on their morphological characteristics and their lack of response to high extracellular potassium (35 mM). Data were calculated as changes in fluorescence ratio and expressed as $\Delta F/F_0$.

2.8. Synaptosomes

Male adult Wistar rats (200–250 g) were euthanized by cervical dislocation and decapitation. The cortex was removed and homogenized in 0.32 M sucrose solution containing dithiothreitol (0.25 mM) and EDTA (1 mM). Homogenates were then submitted to low-speed centrifugation (1000 *g* for 10 min) and the synaptosomes were purified from the supernatant by discontinuous Percoll density gradient centrifugation (39,000 *g* for 15 min) (Dunkley et al., 2008). The synaptosome mix was prepared by resuspending the isolated nerve terminals in Krebs–Ringer–HEPES (KRH) solution (124 mM NaCl, 4 mM KCl, 1.2 mM Mg_2SO_4, 10 mM glucose, 25 mM HEPES, pH 7.4) to a final concentration of approximately 1 mg/mL of synaptosomal protein. Aliquots of 30 µL of the synaptosome mix were pipetted per well of a 96-wells plate and kept on ice until use.

2.9. L-glutamate release

Glutamate release was assessed by measuring the increase in fluorescence due to the production of NADPH in the presence of glutamate dehydrogenase and $NADP^+$, as described previously (Lomeo Rda et al., 2014). Briefly, a mixture of rat cortical synaptosomes (± 30 µg of protein/well) and $NADP^+$ (1 mM) in KRH solution containing 2 mM $CaCl_2$ was transferred to a 96-wells plate (300 µL per well). The plate was placed in a spectrofluorimeter (Synergy 2, Winooski, USA) and readings were continuously performed for 45 min at 37 °C, and 340 nm/440 nm excitation/emission wavelengths. Glutamate dehydrogenase (35 units per well) was added to the wells one minute after the experiment started and fluorescence readings were carried out for 10 more minutes for baseline acquisition. Subsequently, JBU at different concentrations was applied to the wells containing the synaptosomal suspension and the fluorescence readings continued for 45 min. Calibration curves were done in parallel by adding known amounts of glutamate to the reaction medium. The experimental data were expressed as nmol of glutamate released per mg of synaptosomal protein.

2.10. Hippocampal slices

Mice or rats were sacrificed by cervical dislocation and decapitation. Their brains were removed immediately, and the hippocampi dissected out on ice and humidified in cold HEPES-saline buffer (124 mM NaCl, 4 mM KCl, 1.2 mM $MgSO_4$,12 mM glucose, 1 mM $CaCl_2$, and 25 mM HEPES, pH 7.4) gassed with O_2. Coronal hippocampal slices (400 µm thick) were cut using a vibroslicer (MA752, Campden Instruments, USA) or a McIlwain tissue chopper and used to evaluate cytotoxicity of ureases (MTT test) or for electrophysiological recordings (long term potentiation).

2.11. Spontaneous action potential firing in hippocampal slices

The protocols were adapted from Costa-Ferro et al. (2010). Briefly, for extracellular electrophysiological recordings individual hippocampal slices were placed in a submersion-type recording chamber, which was continuously perfused with oxygenated (95 % O_2 plus 5% CO_2) Ringer (composition in mM: NaCl 130, KCl 3.5, NaH_2PO_4 1.3, $MgCl_2$ 2, $CaCl_2$ 2, D-glucose 10, $NaHCO_3$ 24, pH 7.4), at a flow rate of 3 $mL.min^{-1}$. Spontaneous firing of action potentials (responses obtained to 0.05 Hz paired-pulse stimuli, 0.2 ms) was recorded during 20 min in the pyramidal layer of the CA_1 hippocampal region using an Axoclamp 2-B amplifier (Axon Instruments, Foster City, CA, USA) and recorded on a computer using the Axoscope 9.2 software (Axon Instruments). The frequency of action potentials was expressed as the number of events per minute.

2.12. Cell viability assay

Mice hippocampal slices were preincubated at 37 °C for 30 min in HEPES saline (200 µL/slice) in microplate wells (Vinade and Rodnight, 1996). Subsequently, fresh medium was replaced (200 µL/slice) for the control condition or medium containing JBU (0.01, 0.1 and 1 µM), followed by incubation for 1 h (37 °C). JBU-treated slices were assayed for a 3-(4,5-dimethylthiazol-2-yl)-2,5-diphenyltetrazolium bromide (MTT) test (0.05 % in HEPES-saline) for 30 min (37 °C). The water soluble MTT salt is converted into water insoluble purple formazan crystals after cleavage of the tetrazolium ring by mitochondrial dehydrogenases

(Cordova et al., 2004). After 30 min, the hippocampal slices were removed from the wells, the formazan crystals were dissolved in DMSO, and quantified by absorbance at $\lambda = 550$ nm (Liu et al., 1997).

2.13. Ex vivo recordings of compound action potentials from mouse sciatic nerve preparation

Sciatic nerves were obtained from adult male Swiss mice (28–35 g). The extraction surgery was performed essentially as described by Bala et al. (2014). The mice sciatic nerves were mounted on a recording chamber according to Dal Belo et al. (2005). Standard extracellular recording techniques were used to record compound nerve action potentials. Pellet-type silver electrodes were dipped into each of the three compartments of the recording chambers, with stimulation occurring between the central and one of the external compartments. Recordings were obtained from the central compartment. A Grass S48 stimulator was used to supply supramaximal electrical impulses (0.4 Hz, 0.04 ms duration) via a model SIU 5A stimulus isolation unit (Grass Instrument Co.). The signals were amplified with a CED1902 transducer (Cambridge Electronic Design, Cambridge, England), digitalized with a CED 1401 analogue-to-digital converter (Cambridge Electronic Design) and analyzed with custom built software (Dempster, 1993). In each experiment, the amplitude, rise time, latency and threshold of the recorded action potentials were measured. Before adding the test compounds, the sciatic nerve preparations were incubated in physiological solution for 15 min under constant supramaximal stimulation to demonstrate viability of the preparation and consistency of the recordings.

2.14. Long term potentiation (LTP)

2.14.1. In vivo urease treatment

Mice were injected *i.p.* with 2 LD_{50} of CNTX (6.6 mg kg of animal body weight), and immediately after they had the first seizure (around two hours after injection), they were euthanized. Control animals were injected with saline. Mice were decapitated and their brains were removed and stored briefly in ice-cold Ringer solution. Hippocampal slices (400 μm thick) were cut and kept for 60 min in oxygenated (95 % O_2 plus 5% CO_2) Ringer at room temperature before the LTP experiments. The slices were perfused with artificial cerebrospinal fluid (ACSF, composition in mM: NACl 119, $NaHCO_3$ 26, KCl 2.5, NaH_2PO_4 1, $CaCl_2$ 2.5, $MgCl_2$ 1.3, glucose 10, pH 7.4) at a flow rate of 2.0 $mL.min^{-1,}$ for 10 min for baseline acquisition, and then submitted to the tetanic stimulation protocol.

2.14.2. In vitro urease treatment

Hippocampal slices obtained from non treated rats were used for the LTP experiments. After 10 min of baseline acquisition, the slices were perfused with ACSF alone or JBU (1 μM or 0.1 μM) diluted in ACSF, at a flow rate of 2.0 $mL.min^{-1,}$ for 10 min, and then submitted to the tetanic stimulation protocol.

2.14.3. Field excitatory postsynaptic potentials recordings

The protocols were adapted from Costa-Ferro et al. (2010). Field excitatory postsynaptic potentials (fEPSP) were triggered by electrical stimulation of the Schaffer collaterals with constant-current pulses of 0.2 ms duration, delivered every 20 s (0.05 Hz) using a differential alternating current stimulator (Isoflex M.P.I., Israel). The stimulation electrode consisted of a twisted bipolar pair of 75 μm platinum–iridium wire (A-M Systems, Carlsborg, WA, USA). fEPSPs were recorded extracellularly on the pyramidal layer of the CA_1 hippocampal region using an Axoclamp 2-B amplifier (Axon Instruments, Foster City, CA, USA). fEPSPs were amplified and low-pass filtered at 600 Hz (Cyber Amp 320, Axon Instruments), digitalized (Digidata 1322A, Axon Instruments) and recorded on a computer using the Axoscope 9.2 software (Axon Instruments). The amplitude of fEPSPs was measured using the Clampfit 9.2 software (Axon Instruments). At the beginning of each recording, an input–output (I/O) curve for the fEPSP amplitude relative to the stimulus intensity was recorded, using 50 μA stepwise increases (ranging from 50 to 250 μA) until saturation of the fEPSP amplitude. Current intensity was then adjusted to evoke a baseline fEPSP amplitude ranging from 50 to 60 % of the maximal fEPSP amplitude obtained from the I/O curve. Baseline responses obtained to 0.05 Hz paired-pulse stimuli (0.2 ms) were recorded for 20 min before the induction of long-term potentiation (LTP). After reaching stable baseline fEPSP recordings, LTP was induced using a high-frequency stimulation protocol, consisting of four trains of 1 s duration delivered at 100 Hz frequency, with an inter-train interval of 20 s. fEPSPs were monitored for 60 min after tetanic stimuli. Recorded values were normalized on a per recording basis and then plotted as the mean of 2-min time intervals (6 fEPSPs ± S.E.M.) corresponding to two to four slices per experimental animal.

2.15. Heterologous expression of ion channels in Xenopus laevis oocytes

The following Voltage Gated Sodium Channels (VGSCs) were expressed: rNaV1.1, rNaV1.2, rNaV1.3, rNaV1.4, hNaV1.5, mNaV1.6, rNaV1.8 (from rat, mouse of human origin, thus vertebrates) alongside with the insect sodium channel BgNaV (from the cockroach, an invertebrate). Likewise, the following Voltage-Gated Potassium Channels (VGPCs) were investigated: rKV1.1, rKV1.2, rKV1.4, rKV1.5, Shaker IR, rKV2.1, hERG. Furthermore, the voltage gated T-type calcium channels rCav3.1 and rCav3.3 and the nicotinic acetylcholine receptors rα4β2 and rαβγδ (all from rat origin) were also studied in *Xenopus* oocytes. From each cDNA, the linearized plasmids were transcribed using the T7 or SP6 mMESSAGE-mMACHINE transcription kit (Ambion, USA). Oocytes of stage V-VI were extracted from anesthetized *X. laevis* frogs according to Liman et al. (1992). Oocytes were then injected with 50 nL of cRNA at 1 $ng.nL^{-1}$, using a micro-injector (Drummond Scientific, Broomall, PA, USA). The oocytes were incubated in a solution containing 96 mM NaCl, 2 mM KCl, 1.8 mM $CaCl_2$, 2 mM $MgCl_2$ and 5 mM HEPES (pH 7.4) and supplemented with 50 mg/L gentamycin sulfate.

2.16. Voltage-clamp recordings

Two-electrodes voltage-clamp recordings were performed at room temperature (18–22 °C) as described by Peigneur et al. (2019), using a GeneClamp 500 amplifier (Molecular Devices, USA), controlled by a pClamp data acquisition system (Axon Instruments, USA). Whole cell currents from oocytes were recorded 1–4 days after cRNA injection. Bath solution was ND-96 (composition: 96 mM NaCl, 2 mM KCl, 1.8 mM $CaCl_2$, 2 mM $MgCl_2$ and 5 mM HEPES [pH 7.4]). Voltage and current electrodes were filled with 3 M KCl. Resistances of both electrodes were kept between 0.7 and 1.5 MΩ. The elicited currents were sampled at a frequency of at least double the filtering frequency, using a 4-poles low-pass Bessel filter. Leak subtraction was performed using a -P/4 protocol. Currents were evoked by 250 ms depolarizations to 0 mV, followed by a 250 ms pulse to −50 mV from a holding potential of −90 mV, that was recorded as one sweep. After five or six control sweeps, CNTX (1 nM, 10 nM, 100 nM, 1 μM) was pipetted into the measuring bath containing the oocyte, and the recordings proceeded for approximately ten more sweeps. In order to investigate the current-voltage relationship, current traces were evoked by 5 mV depolarization steps from a holding potential of −100 mV. For acetylcholine receptors recordings, three pulses of 100 μM acetylcholine were manually applied during perfusion, then a 1 μM CNTX pulse was applied, and at the end, three additional acetylcholine pulses were given. The leak current was recorded. Data represent independent experiments of at least three experiments ($n \geq 3$).

2.17. $^{[18F]}$Fluorodeoxyglucose micro positron emission tomography ($^{[18]}$FDG-microPET

For $^{[18]}$FDG microPET scans, all animals were fasted for 12−24 hours

to increase the ^{18}FDG uptake in the brain. The rats were kept on a heating pad at 36 °C for 30 min before CNTX injection. They were removed from their cages, anesthetized with isoflurane mixed with oxygen (3–4 % v/v) and injected with 37 MBq of ^{18}FDG i.p. and with 0.625LD$_{50}$ of CNTX e.v., or 37 MBq of ^{18}FDG + vehicle (controls). The animals were then returned to their cages for 40 min to allow conscious ^{18}FDG uptake. After the tracer uptake period, rats were again anesthetized with inhaled isoflurane mixed with oxygen (3–4% for anesthetic induction and 2–3% for anesthesia maintenance). The animals were placed in a headfirst prone position and scanned on a Triumph™ microPET apparatus (LabPET-4, TriFoil Imaging, Northridge, CA, USA). Throughout these procedures, animals remained at a controlled temperature of 36 °C. For radiotracer readings, 10-min list mode static acquisitions were performed with the field of view (FOV; 3.75 cm) centered on the rat's head. All data were reconstructed using the maximum likelihood estimation method (MLEM-3D) algorithm with 20 iterations. Each reconstructed microPET image was spatially normalized into an ^{18}FDG template using PMOD v3.5 and the Fusion Toolbox (PMOD Technologies, Zurich, Switzerland). An MRI rat brain volume of interest (VOI) template was used to overlay the normalized images, previously coregistered to the microPET image database. The ^{18}FDG uptake in the whole brain, hippocampus, thalamus, pons and medulla oblongata were normalized for the injected dose and body weight. The standardized uptake value (SUV) was calculated for the whole brain and each individual region. In order to correct for weight variations, the SUV ratio (SUVr) of each individual brain region was calculated dividing the SUV value of the region by the whole brain SUV (Baptista et al., 2015; Saur et al., 2017; Zanirati et al., 2018).

2.18. Statistical analysis

Results are presented as mean ± standard error of the mean (SEM). One-way analysis of variance (ANOVA), followed by the LSD post-hoc test, was used for fEPSPs data, voltage clamp data and the whole brain data analysis in microPET experiments. Prism GraphPad (version 6.0, GraphPad Software Inc, San Diego, California) was used for the analysis. Graphs were made using either Prism GraphPad (version 6.0, GraphPad Software Inc, San Diego, California) or Origin (version 9.0, OriginLab Northampton, Massachusetts, USA). Statistical differences were considered significant when $p < 0.05$.

3. Results and discussion

The major aim of this work was to gain novel information about the neurotoxic mechanisms of CNTX and JBU, especially those associated to triggering of epileptogenic events in rodent models. Therefore, the present study also aided in the risk assessment of *C. ensiformis* ureases and other potentially neurotoxic microbial ureases. Here, either CNTX or JBU were used for the experiments according to the availability, except for *in vivo* protocols requiring intraperitoneal administration, in which case CNTX was used. Rats and mice were used as experimental models. Twenty years after CNTX was first isolated, it was characterized as an isoform of JBU (Follmer et al., 2001), differing from the latter mainly in its smaller molecular size, reflecting a different oligomerization state in solution, i.e. JBU is a hexamer of 540 kDa while CNTX behaves mostly as a dimer with 185 kDa. Except for intraperitoneal toxicity in rodents, which is observed only for CNTX (both isoforms are equally active if given by intravenous route), all other known biological properties tested for both ureases occur in similar dose or concentration ranges (Carlini and Ligabue-Braun, 2016). In some bioassays, CNTX is capable to induce effects at doses 20–30 % lower than those observed for JBU. The lack of neurotoxicity of JBU given by intraperitoneal route probably reflects its higher molecular mass impacting the pharmacokinetics and biodistribution of the toxin.

Seizures consists of rapid, synchronous and uncontrolled propagation of electric potentials throughout the brain, which constitutes the bases of the convulsive phenomenon (Cornes et al., 2014). The mammalian nervous system has two important mechanisms to prevent convulsions: 1) at cellular level, the refractory period induced by hyperpolarization of voltage gated sodium channels, and 2) the blockade produced by neural networks mediated by gabaergic interneurons, which promote chloride ions influx to cause hyperpolarization of the post-synaptic neuron, thus making less likely the firing of an action potential (Bezanilla, 2006; Rang et al., 2016). Our group established the central nervous system as the target for CNTX's convulsant effect (Carlini et al., 1984). Seizures of rat hind limbs persisted, although somewhat delayed, after spinal section at T7 level. Moreover reserpine, a drug that inhibits the vesicular transport of monoamines, reduced the threshold of CNTX-induced seizures in rats (Carlini et al., 1984).

Here, in an attempt to understand the mechanism of neurotoxic action induced by *C. ensiformis* ureases, a number of *in vivo*, *ex vivo* and *in vitro* bioassays were conducted.

3.1. Electroencephalographic (EEG) recordings

An intrahippocampal injection of JBU (0.018 μg.kg^{-1}) induced a 3 Hz generalized spike-wave discharge (Fig. 1). This finding suggested a non-convulsive "*petit mal*" seizure, as the animals did not respond to external sound stimulation nor presented tonic-clonic convulsions (Loiseau, 1992; Snead, 1995).

Spike-and-wave is the term that describes a particular pattern of the electroencephalogram (EEG) usually seen during epileptic seizures. The spike-and-wave discharge is a regular, symmetrical, generalized EEG pattern generally associated to absence '*petit mal*' epilepsy (Loiseau, 1992). The basic mechanisms underlying these patterns are complex and involve part of the cerebral cortex, the thalamocortical network, and intrinsic neuronal mechanisms (Snead, 1995). Some studies suggested that a thalamocortical loop is involved in the initiation of spike-and-wave oscillations (Akman et al., 2010; Fan et al., 2016; Snead, 1995; Zhang et al., 2015). Studies on thalamic brain slices suggested that inhibition of thalamic relay neurons by GABA-ergic interneurons hyperpolarizes the relay neuron, thus removing inactivation of T-type Ca^{2+} channels (McCormick and Contreras, 2001). This sequence of events leads to a rebound burst of action potentials after each inhibitory post-synaptic potential (IPSP). The action potential stimulates the GABAergic neurons by a reciprocal excitatory connection. The action potentials in the relay neurons also excite cortical neurons, appearing in the EEG as a "spindle" (McCormick and Contreras, 2001). In our experimental conditions, JBU was injected directly into the rat hippocampus, from where SWDs originated in CA_1 were propagated to mPFC and TMD, 45 min after the injection. This latter result suggests that JBU induces an intense hypersynchronous burst firing activity in the CA_1 area that caused the electrical activity to spread to other brain regions. There is a striking link between the involvement of T-type calcium channels in the CA_1 area of the hippocampus and the development of SWDs (Iftinca, 2011). Calcium influx through verapamil-inhibitable channels has been previously observed during the course of platelet activation promoted by CNTX (Ghazaleh et al., 1997).

3.2. JBU induced Ca^{2+} events in rat hippocampal primary cultures

Perfusion in rat hippocampal primary cultures with JBU (0.1 μM) increased intracellular calcium levels (Fig. 2), with rise in the action potential firing rate (Fig. 3B).

JBU (0.001−1μM) increased $[Ca^{2+}]_I$ in rat primary hippocampal cultures at all concentrations tested. In this set of experiments, the individual analysis of the cells indicated that only some specific neurons were activated, as indicated by the KCl (35 mM) perfusion used to identify astrocytes (Fig. 2E). An inverted dose-response curve was observed for the effect of JBU on calcium events. JBU (1 μM) led to an increase in the $[Ca^{2+}]_i$ of 350 ± 20 % (n = 90 cells, $p < 0.05$ compared to vehicle) while the lowest concentration of JBU promoted an increase in

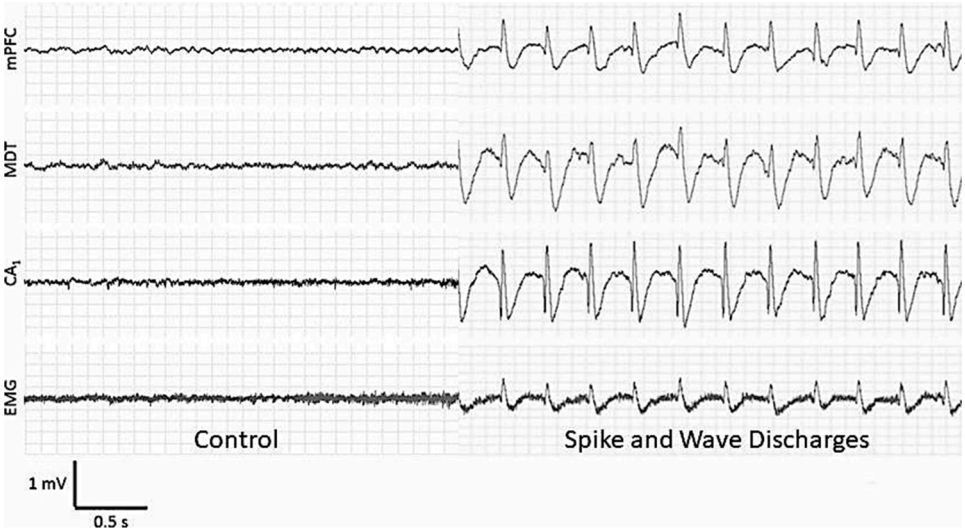

Fig. 1. Electroencephalographic recordings (EEG) in a rat showing an absence-like epileptical activity induced by Jack Bean Urease (JBU). The recordings show typical waveforms from the medial pre-frontal cortex (mPFC), medium dorsal nucleus of the thalamus (MDT), CA_1 region of the hippocampus and an electromyogram (EMG), during the onset of JBU's effect. Note the spike-wave waveforms in all recordings. The hypersyncronous low frequency spike-and-wave discharges signal was so intense and generalized that it was also recorded on the EMG. The criterium for SWDs analysis was that they should last at least 3 s. Typical result.

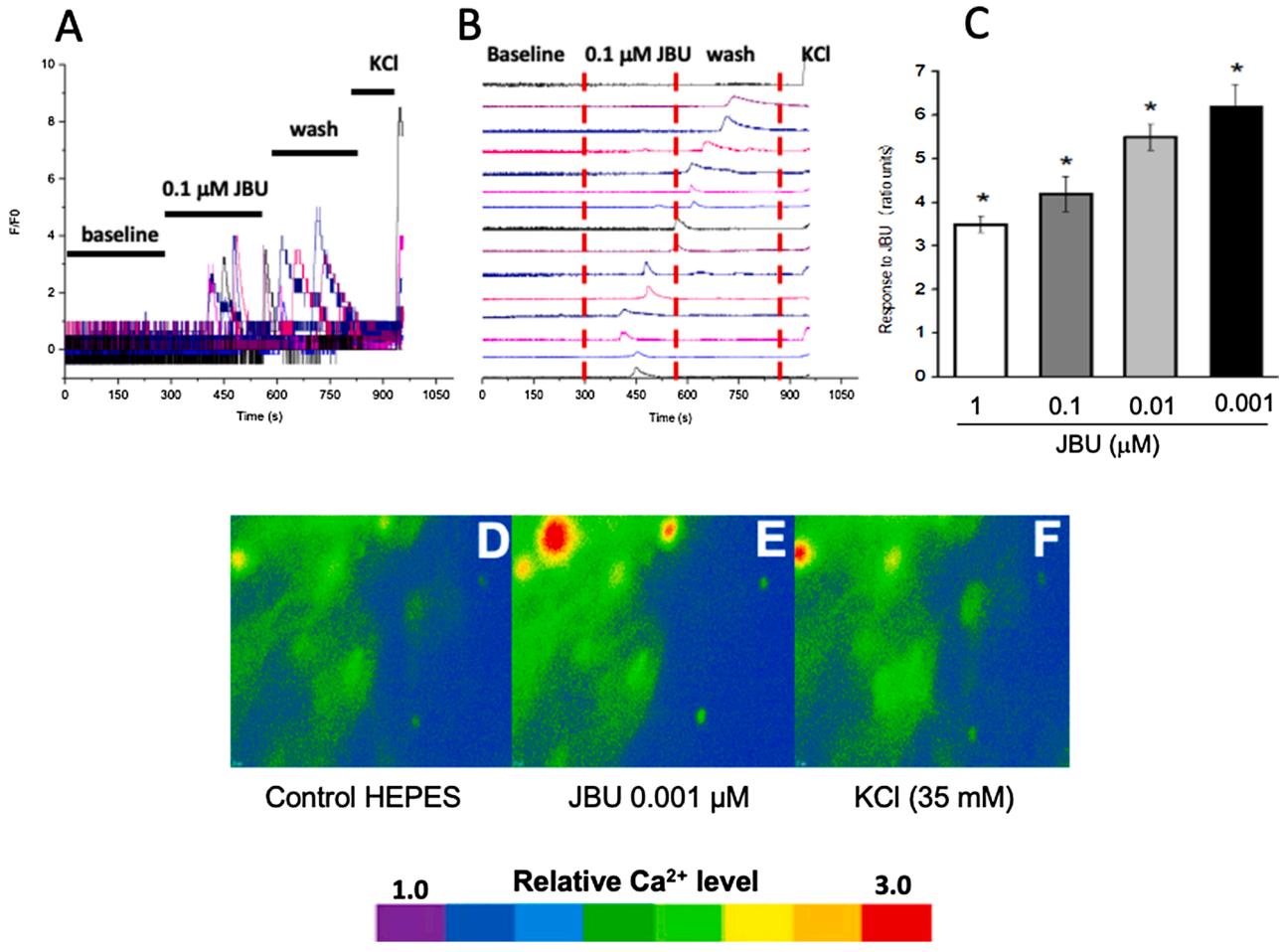

Fig. 2. JBU increases intracellular levels of calcium in rat hippocampal primary cultures. Panel A) The graph illustrates superimposed fluorescence tracings of $[Ca^{2+}]_i$ kinetics in individual hippocampal neurons (different colors) before (baseline), during perfusion with JBU (0.1 µM), during wash (perfusion without JBU), and after addition of 35 mM KCl. Panel B) Individual tracings of the 14 cells selected for analysis of $[Ca^{2+}]_i$ kinetics. Control cell (top tracing) was not treated with JBU while the others were perfused with JBU (0.1 µM) during the 300-570 s interval. Addition of 35 mM KCl to the perfusate was performed at 870 s. Note that the application of JBU elicits transitory spikes of calcium influx and cells remained in an activated state after washing out the urease. Panel C) Dose-response effect of JBU on the levels of intracellular calcium of rat hippocampal primary cultures. Panels D, E and F) show the increased $[Ca^{2+}]_i$ in hippocampal neural cells loaded with FLUO-4 AM after treatment with JBU. The panels show representative pseudocolour images of calculated calcium influx at resting state (control, HEPES), in the presence of JBU 0.1 µM (D) or with HEPES-Saline with KCl 35 mM (E).

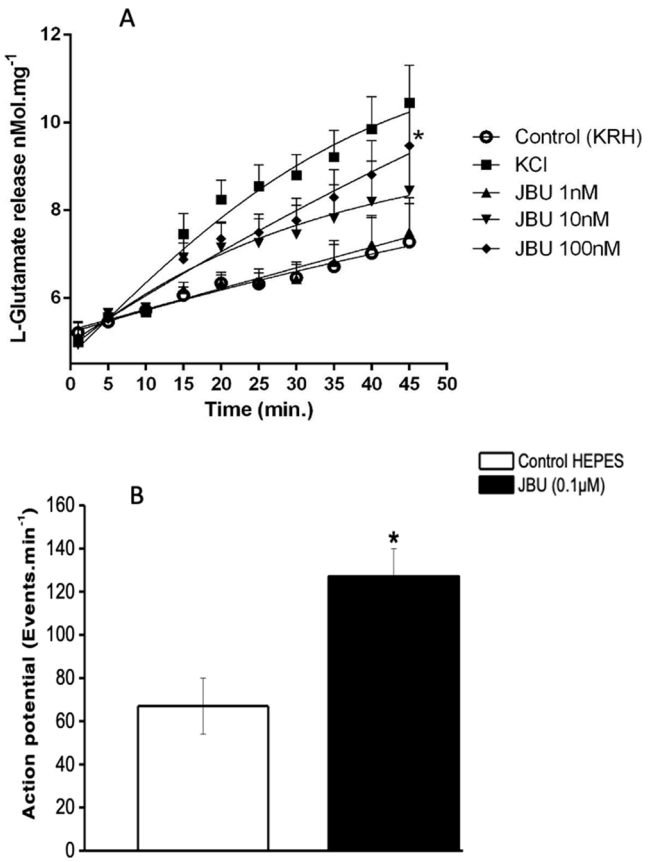

Fig. 3. L-glutamate release in rat synaptosomes and excitatory action of JBU in rat brain hippocampus. Panel A) a mixture containing synaptosomes (±30 mg of protein/well) and $NADP^+$ (1 mM) in KRH (Krebs Ringer solution) was transferred to microplates (300 mL/well) coupled to a spectrofluorimeter (Synergy 2), set at 340 nm/440 nm excitation/emission wavelengths. After 1 min of blank reading, glutamate dehydrogenase (35 units/well) was added and the baseline acquisition continued for 10 min. Subsequently, JBU (1, 10 and 100 nM) or KRH (control) or KCl (33 mM; positive control) were added and the readings continued for 45 min. Data are mean ± S.E.M., n = 6 (*$p < 0.05$). Panel B) JBU increases the frequency of spontaneous action potentials on hippocampal CA1 area. The graph shows the increase of action potentials recorded per minute when brain slices are perfused with 0.1 μM JBU compared to the control condition (*$p < 0.05$). Mean ± S.E.M., N = 4.

the $[Ca^{2+}]_i$ of 650 ± 50 % (n = 90 cells, $p < 0.05$). Similar inverted dose-effect curves have been previously observed for other biological activities of JBU (Staniscuaski et al., 2009). We have also demonstrated, that in concentrated solutions, JBU oligomerizes to form soluble inactive aggregates (Follmer et al., 2004a), thus it is plausible that larger doses of the protein, which required concentrated solutions to be achieved, could be less effective.

Another possibility to explain the inverted dose-effect curve is if JBU is acting like an inverted agonist. In such a condition, the activity related to the binding of the protein to an active receptor with a higher affinity would be counteracted by a higher urease concentration binding to a lower affinity, inactive form of the receptor (Milligan, 2003).

Although we have not addressed which type of calcium channel is involved in the JBU-induced increase of calcium influx in the hippocampus, it is possible that T-type calcium channels are activated by the toxin, which would agree with the appearance of SWDs in the rat brain. The large conductance calcium-activated potassium (BK) channel is also considered as a vital player in the pathogenesis of epilepsy, regulating the shape and duration of action potentials (Zhu et al., 2018). BK channels are expressed widely in neurons, and membrane depolarization and intracellular Ca^{2+} levels regulate their activation. BK channels are functionally coupled to both voltage-gated Ca^{2+} channels (VGCCs) (e.g. T-type calcium channels) and channels mediating Ca^{2+} release from intracellular stores (e.g. ryanodine receptor (RyR)–mediated intracellular Ca^{2+} release) (Whitt et al., 2018).

3.3. JBU induces release of L-glutamate from rat synaptosomes

The effect of JBU was evaluated on the release of L-glutamate (L-Glu), the most important excitatory neurotransmitter in mammalian CNS. L-glutamate plays a critical role in epileptogenesis, in the initiation and spreading of seizures (Meldrum, 1994). It has been shown that in a twelve-day hippocampal culture, neurons normally express markers for either L-Glu (~ 90 % of neurons) or GABA (~ 10 % of neurons) neurotransmitter systems (Bengtson et al., 2013). Here we show that JBU (0–100 nM) induced a significant concentration- and time-dependent release of L-Glu (n = 6) from rat brain synaptosomes (Fig. 3A). Thus, in synaptosomes exposed to 10 nM JBU for 45 min, a tendency to the release of L-Glutamate was already seen. In the presence of 100 nM JBU, released L-Glu was 9.46 ± 0.97 nanomols.mg^{-1}. min^{-1}, an increase of 33.3 ± 8.5 % compared to controls (7.27 nanomols.mg^{-1}. min^{-1} ± 0.87, $p < 0.05$). This response corresponded to 90.7 % of that observed in depolarizing conditions (KCl) assayed in parallel.

Previous studies have shown that 500 nM CNTX induced release of ^{3}H-serotonin and ^{3}H-dopamine from preloaded rat brain synaptosomes (Barja-Fidalgo et al., 1991b). No significant level of lactate dehydrogenase was detected in the medium, indicating CNTX did not induce lysis of the synaptosomes. The amounts of neurotransmitters released by CNTX were equivalent to that obtained by depolarizing the synaptosomes with KCl. The exocytosis-inducing effect of CNTX was lipoxygenase-dependent whereas the release of neurotransmitters from KCl-depolarized synaptosomes was only mildly inhibited by the lipoxygenase inhibitor, nordihydroguaiaretic acid (Barja-Fidalgo et al., 1991b). Other studies of our group have shown that JBU is able to modulate calcium influx and to induce depletion of intracellular L-glutamate in insect neuromuscular junctions (Carrazoni et al., 2018).

3.4. JBU increases the frequency of action potentials of pyramidal neurons in rat hippocampus

Consistent with the effect of JBU in releasing the excitatory neurotransmitter L-glutamate, an increase of the spontaneous firing rate of pyramidal neurons was registered in the CA1 region of rat hippocampus slices after 2 min of perfusion with the urease at 0.1 μM concentration (Fig. 3B). Increase of frequency of action potentials was also seen in rat primary hippocampal cultures perfused with JBU (data not shown). This result agrees with the observed spike and discharge pattern observed in the CA1 region of hippocampus of JBU-injected rats, as seen in Fig. 1.

3.5. JBU does not affect mice hippocampal cell viability

The eff ;ect of different concentrations of JBU (0.001−1μM) on cell viability was evaluated on mice hippocampal slices by using the MTT assay. In this set of experiments, the incubation of the tissues with H_2O_2 (44 mM) reduced in 80 % the cell viability (n = 6, $p < 0.05$), when compared to the control (incubation with HEPES-saline). On the other hand, JBU did not affect the cell viability of mice hippocampus in any of the tested concentrations (Suppl. Fig. 2).

Similar observations of lack of cytotoxicity or of lytic effect were made for CNTX in most of the *in vitro* cellular assays performed with this urease, in doses up to 500 nM – 1 μM, such as in platelets (Carlini et al., 1985), macrophages and monocytes (Barja-Fidalgo et al., 1992), mast cells (Grassi-Kassisse and Ribeiro-DaSilva, 1992), pancreatic β-cells (Barja-Fidalgo et al., 1991b, 1991a). No lytic effect was observed in CNTX-treated synaptosomes which had undergone release of neurotransmitters (Barja-Fidalgo et al., 1991b). Although JBU was shown to insert itself into the lipid bilayer of liposomes (Micheletto et al., 2016)

and to form ion channels when inserted into planar lipid bilayers (Piovesan et al., 2014), this membrane-disturbing property does not cause lysis, as cells exposed to the ureases remained viable. The fact that JBU does not affect neuronal cell viability is an indicative that the amount of released L-Glutamate induced by the toxin is probably not cytotoxic to the hippocampal cells. These results allow us to infer that mitochondrial dysfunctions are not associated with the seizure-inducing activity of *C. ensiformis* ureases (Henshall, 2007; Zsurka and Kunz, 2015).

3.6. Effect of JBU on compound action potentials (CAP) of mouse sciatic nerve

Perfusion of the mouse sciatic nerve with JBU caused significant changes in amplitude and rise time of the compound action potentials (CAP). Fig. 4 displays JBU's effect on CAP at different doses. The most significant decrease (~40 %) in CAP amplitude was observed ($n = 6$, $p < 0.05$) for the lowest dose of JBU, 0.001 μM. The "blocking" effect of JBU on the CAPs decreased as higher concentrations of the toxin were employed. For the largest dose tested, 1 μM, JBU inhibited ~5% the amplitude of sciatic nerve's CAPs, after 120 min of incubation. An inverted dose-effect curve was also seen for the increase in [Ca2+]i promoted by JBU (Fig. 2).

The application of tetrodotoxin (TTX, 1 μM), added to the preparation either 120 min after or before JBU, did not alter the urease's inhibitory effect on CAPs (Suppl. Fig. 1), indicating that the inhibition promoted by the toxin could be due to an effect on tetrodotoxin-sensitive voltage gated sodium channels. It is worth noting that Ca^{2+} events in the sciatic nerve depend on voltage-gated Na + channels that are TTX-sensitive (Deshpande, 1998).

In the CAP experiments, the partial inhibition of the potentials' amplitude could indicate that JBU is not a specific sodium channel blocker. Therefore, at a central level it is also possible that JBU could interfere on sodium currents from excitatory and inhibitory neurons at the same time, causing a detrimental effect on central nervous system similar to lidocaine, that in small doses produces inhibition in the CNS and in higher doses, produces excitation (Onizuka et al., 2005).

The compound action potential is the algebraic summation of action potentials from all neurons in a nerve. Some fibers fire faster than others creating a U-shaped curve. Besides an effect of JBU in promoting partial inhibition of voltage-gated Na^{+} channels, what appears to be a CAP blockade caused by JBU could be a destructive interference of neurons firing dyssynchronously resulting in a change of phase in neural rhythm (Mortimer and Badra, 2003). Changes of phase also occur in seizures due to disturbances in the natural neural rhythms of the brain, as is the case of "*petit mal*" seizures seen in the EEG experiments (Fig. 1), which are triggered by excessive calcium influx (Rang et al., 2016).

3.7. Ureases affect long term potentiation

3.7.1. In vivo effect of CNTX

Hippocampal slices of mice that were injected i.p. with 2 LD_{50} CNTX were not able to induce LTP after tetanic stimulation (Fig. 5A). Induction of LTP is considered positive if fEPSP amplitude after tetanic stimulation increases at least 40 % compared to the baseline. The inhibition of LTP in hippocampal slices or CNTX-treated mice persisted during the 60 min observation interval as opposed to hippocampal slices of control animals, which sustained LTP throughout the same period.

3.7.2. In vitro effect of JBU

Treatment of rat hippocampal slices *in vitro* by perfusion with JBU affected LTP induction as well, in a time and concentration-dependent manner. Perfusion of slices with JBU (1 μM) significantly impaired short-term potentiation, as induction of LTP occurred only 30 min after the high-frequency stimulus train (Fig. 5B).

Hedou and co-workers (Hedou et al., 2008) found that long term potentiation and depression are mechanisms that could be involved in brain recovery and also in brain damage. In the same study, it was demonstrated that the neuroprotective effects of the enzyme protein phosphatase 1 (PP1) on the oxygen glucose deprivation (OGD) model of ischemia are coupled to long term depression. Pharmacological or genetic inhibition of PP1 and inducing LTP before OGD cause brain damage, which was verified by impaired fEPSP recovery. Since CNTX induces hypoxia (Ribeiro-DaSilva et al., 1989) and hypoglycemia (Ribeirodasilva and Prado, 1993), these facts allow us to infer that a neuroprotective mechanism such as PP1 activation could take place to counteract CNTX's neurotoxic effect.

Also, LTP is a form of neuronal plasticity that strengthens connections between presynaptic and postsynaptic neurons in a persistent way. This plasticity is very similar to the one present in kindling models of epilepsy in which convulsions are induced by high frequency electrical stimulation of the perforant pathway. The recurrent convulsions caused by this model decrease the seizure threshold due to a use-dependent

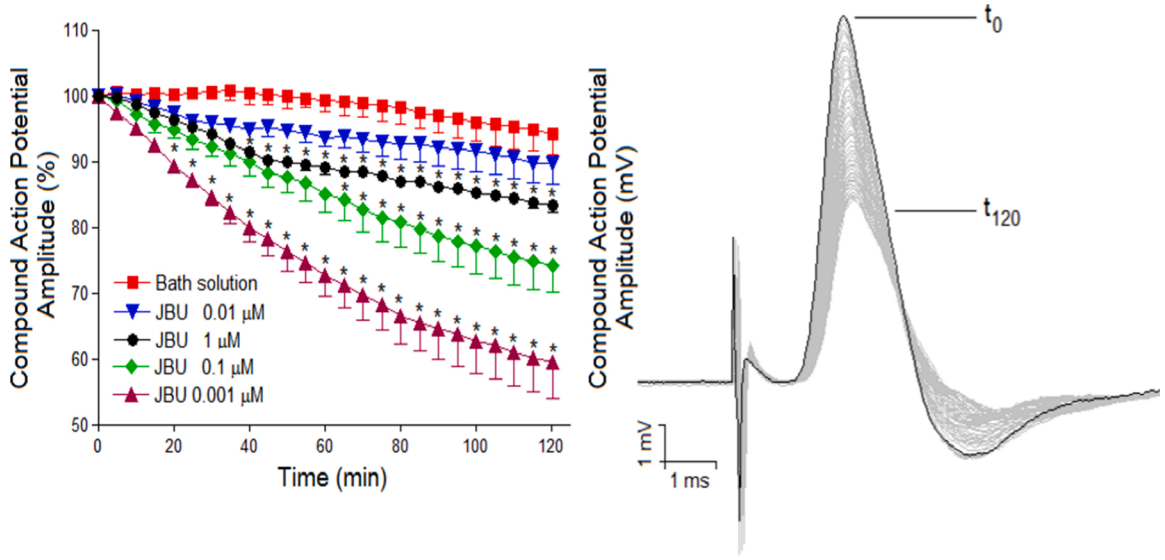

Fig. 4. Measurements of the compound action potential recorded in mouse sciatic nerve. A. The graphic displays the decrease observed in CAP amplitude during incubation with JBU (0.001-1 μM, $n = 3$). B. Representative superimposed records of a preparation treated with JBU 0.001 μM. In A, *$p < 0.05$ compared to control preparations.

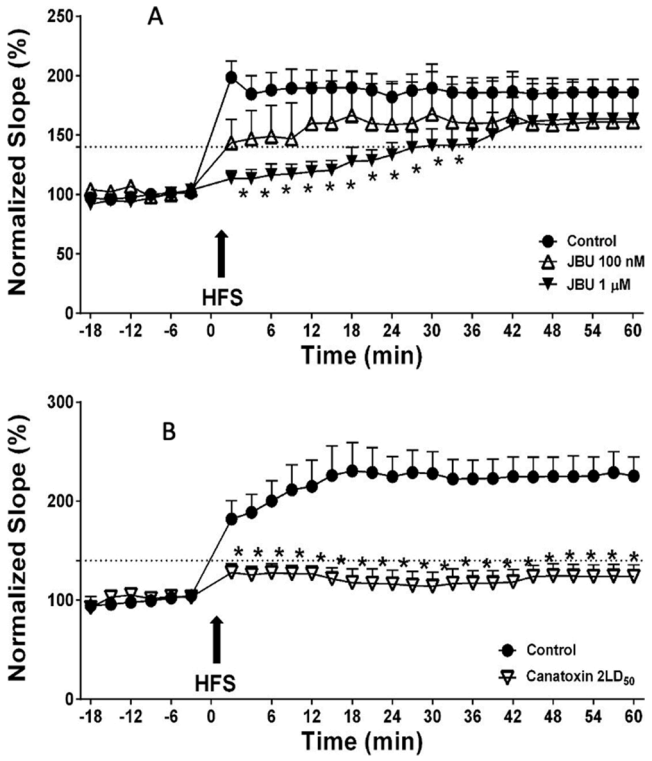

Fig. 5. JBU and Canatoxin affect synaptic plasticity in the hippocampus. After recording a baseline of 20 min, a high frequency stimulation (HFS) protocol was applied to hippocampal slices at 0 min (arrow) and fEPSPs were registered during 60 min afterwards. The criterium for induction of Long Term Potentiation (LTP) is when fEPSPs amplify at least 140 % (dot line) compared to baseline, after tetanic stimulation. Panel A) Perfusion of non-treated rat hippocampal slices with JBU inhibits LTP in hippocampal CA_3-to-CA_1 network. Hippocampal slices of non-treated rats were perfused with medium alone (control) or medium containing 1 µM JBU (squares symbols) or 0.1 µM JBU (open circles symbols) Mean ± SEM, N = 6 (each), * $p < 0.05$. Panel B) Treatment of mice with Canatoxin prevented LTP induction in hippocampal slices. Hippocampal slices were prepared from mice treated with canatoxin (2 LD_{50}). Multiple t-tests indicated that CNTX's data are significantly different from control (* $p < 0.05$) for all datapoints after HFS. Mean ± SEM, n = 9.

NMDA plasticity (Bertram, 2007; Kullmann et al., 2000). Hence both, the long term depression (LTD) observed in hippocampal slices of CNTX-treated mice, and the LTD seen in JBU-perfused slices, could have a neuroprotective role to prevent neuronal damage. This hypothesis is also consistent with our data showing no alteration of cell viability in JBU-treated hippocampal slices (Suppl. Fig. 2)

Another possible explanation for the impairment in LTP induction by the toxins could be the fact that the neurotoxicity by *C. ensiformis* ureases' requires metabolites of the lipoxygenase pathway (Barja-Fidalgo et al., 1988, 1991b). It has been reported that the direct application of 12 (S)-HPETE, an eicosanoid originated in nervous tissues by the action of the 12-lipoxygenase, to hippocampal slices causes a LTD similar to the that mediated by the metabotropic L-Glu receptor (mGluR-LTD) (Feinmark et al., 2003). Normandin and collaborators (Normandin et al., 1996) reported that homosynaptic LTD in hippocampal CA_1 area requires activation of glutamatergic NMDA receptor, changes in postsynaptic Ca^{2+} concentration and phospholipase A_2 (PLA_2) activation. According to the authors, after Ca^{2+}-dependent PLA_2 activation, eicosanoids derived from arachidonic acid released by the action of PLA_2 upon the cell membrane act as intra- and extracellular messengers. This study showed that inhibitors of cyclooxygenases did not prevent LTD, whereas inhibitors of 12-lipoxygenase (12-LO), but not of 5-lipoxygenase, averted LTD induction. The authors concluded that activation of endogenous PLA_2 and formation of 12-LO metabolites are important for LTD induction (Normandin et al., 1996). We have previously reported that the exocytosis-inducing activity of CNTX in platelets and also in synaptosomes depended on PLA_2 and 12-LO activities (Barja-Fidalgo et al., 1988, 1991b; Carlini et al., 1985). Moreover, pre-treatment of rats with the lipoxygenase inhibitor nordihydroguaiaretic acid, prior to injection of CNTX, protected the animals against the toxin-induced seizures (Ribeiro-DaSilva et al., 1989).

3.8. Lack of effects of canatoxin on voltage gated ion channels and acetylcholine receptors

In voltage-clamp experiments, perfusion with CNTX (concentrations ranging from 1 nM up to 1 µM) did not affect the tested subtypes of sodium channels overexpressed in *X. laevis* oocytes (Fig. 6A). CNTX also did not change the kinetics of activation or inactivation of the tested voltage gated sodium channels (Fig. 6B). Moreover, CNTX did not seem to interfere or modulate calcium or potassium currents of the selected voltage-gated channels (Fig. 7A) or the activity of the tested nicotinic receptors (Fig. 7B).

Considering the lack of effect of CNTX in these assays, it should be noted that the overexpression of a single type of ion channel in the *Xenopus* oocyte model is not representative of the complexity of neural networks nor of the interplay of different ion channels in a neuron. Neither were all known subtypes of channels available for tests. Thus, the lack of effect of CNTX on the ion channels tested in this work does not necessarily exclude a possible action of the toxin at this level.

The data, however, goes in line with some of our previous results showing the lack of effect of CNTX on a variety of mammalian as well as on toad neuromuscular junction preparations (Carlini et al., 1984).

The fact that CNTX did not interfere with muscular nicotinic receptor αβγδ (Fig. 7B) matches these results. On the other hand, the lack of CNTX's effects on the CNS nicotinic receptor α4β2 (Fig. 7B) does not discard a central action of the toxin, as there is also glutamatergic and gabaergic neurotransmission that play important roles in epilepsy (Meldrum, 1994; Treiman, 2001).

CNTX had no effect on the T-type voltage gated calcium channels, but this does not preclude previous data showing interference of this urease on calcium influx or transport. Each mammalian cell has about 300 ion channels (Lamothe and Zhang, 2016). Calcium influx accompanying exocytosis in CNTX-activated platelets was shown to occur through verapamil-inhibitable calcium channels (Ghazaleh et al., 1997). Platelets have numerous types of calcium channels activated by second messengers, calcium itself, ATP and other ligands (Mahaut-Smith, 2012; Zschauer et al., 1988). Voltage gated calcium channels, probably of T-type, were characterized in guinea-pig megakaryocytes (platetet precursor cells) (Kawa, 1990). CNTX was also reported to interfere on the calcium transport by rabbit sarcoplasmic reticulum inside-out vesicles. In this system, CNTX inhibited calcium accumulation in the vesicles by interacting with the sarcoplasmic reticulum calcium pump, thereby uncoupling calcium uptake and ATP hydrolysis by the muscle Ca^{2+}/Mg^{2+}- dependent ATPase (Alves et al., 1992). As part of the neurotoxic effect of JBU in insects, the toxin was shown to modulate neurotransmitter release, consequent to an increased calcium influx in presynaptic terminals, hence depleting synaptic vesicles and leading to blockage of neuromuscular junctions (Carrazoni et al., 2018). Reinforcing a potential indirect effect of ureases on ion channels, preliminary results (not shown) of patch-clamp experiments suggested that in rat hippocampal slices perfused with JBU, the toxin seems to alter sodium currents, but not potassium currents. On the other hand, the data gathered so far could also be indicative that the neurotoxic activity of *C. ensiformis* ureases occurs at a neural network level, rather than at a cellular level.

Voltage gated sodium channels (VGSC) are often a therapeutic target for epilepsies (Mantegazza et al., 2010). The $Na_v1.1$ is present primarily in inhibitory GABAergic neurons (Zhang et al., 2019). Mutations causing loss of function of Na_v 1.1 can induce severe untreatable epilepsies

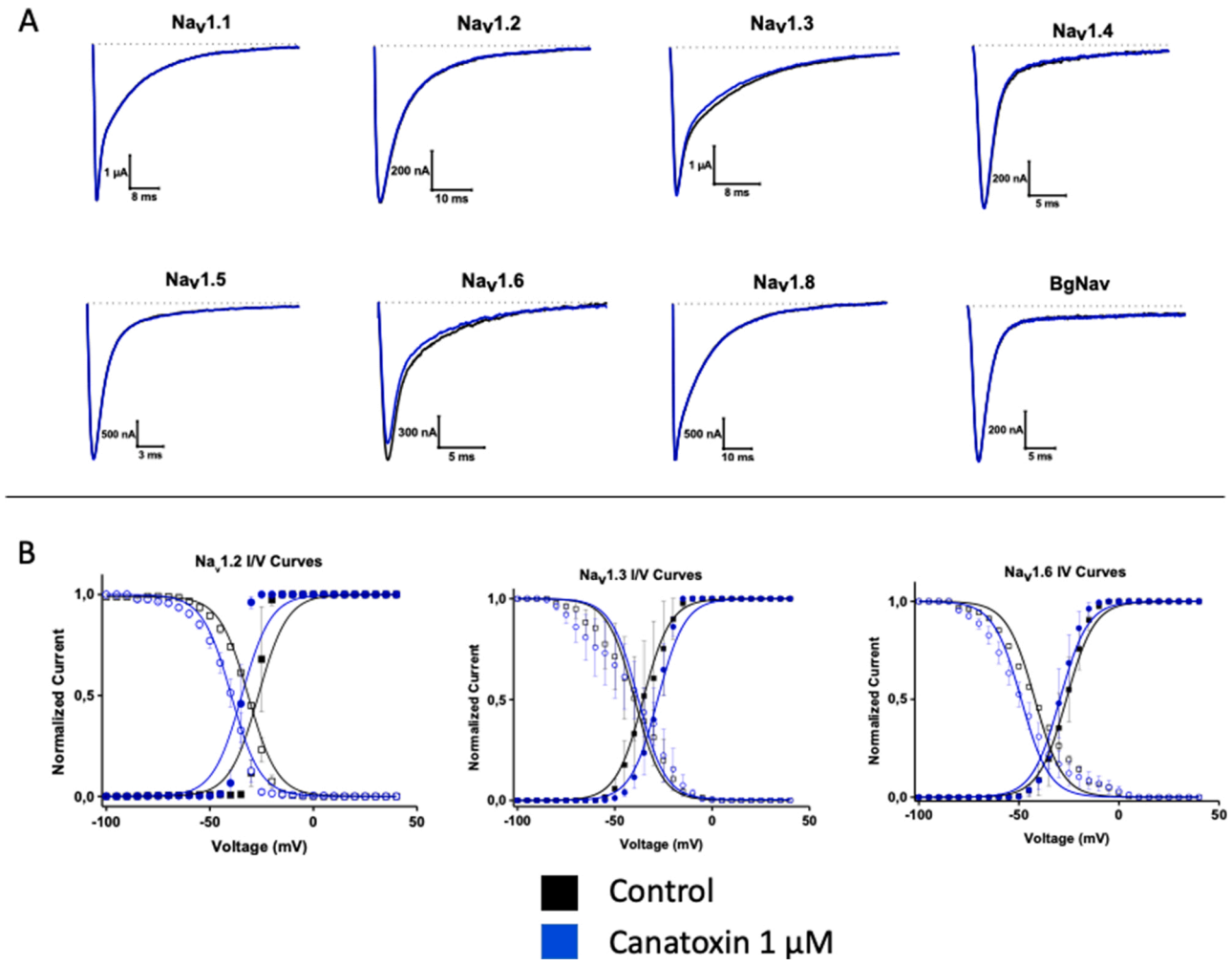

Fig. 6. Screening of Canatoxin effects on selected voltage gated sodium channel *Xenopus* oocytes overexpressing the ion channels were perfused with1 μM CNTX during 15 s at 3 mL.min^{-1}. Panel A) No significant changes in sodium currents were observed in any of the tested channels ($p < 0.05$, $n = 6$). Panel B) Canatoxin did not seem to modulate the steady-state kinetics of activation and inactivation of the tested voltage gated sodium channels. The V_0 values (voltage at which 50 % of the channels are open) did not change significantly when compared to controls in both activation and inactivation ($p < 0.05$, $n = 6$). For all sodium channel activation curves, the K value was > 5. These experiments were repeated at least with two different batches of CNTX.

(Mantegazza et al., 2005). If $Na_v1.1$ currents are blocked, the inhibition in a given neural network is reduced because of impaired GABAergic signaling, so that excitatory neurons would fire excessively causing seizures (Zhang et al., 2019). It has been demonstrated a striking relationship between the neuronal Nav 1.6 and spike wave discharges, the hallmark of epilepsy crises (Papale et al., 2009). The axons of rodent sciatic nerve used in CAP experiments contain tetrodotoxin-sensitive voltage gated sodium channels of the subtypes: $Na_v1.1$, $Na_v1.2$, $Na_v1.3$, $Na_v1.6$ and $Na_v1.7$ (Wilson et al., 2011). Our data showing partial inhibition of CAP in JBU-treated mouse sciatic nerve suggested that JBU is not a specific sodium channel blocker. Unlike the different classes of potassium or calcium channels, the functional properties of the known voltage gated sodium channels are relatively similar (Yu and Catterall, 2004). Individual CNS neurons express multiple VGSC isoforms which are functionally and pharmacologically distinct (Soderlund et al., 2017). Despite the fact that in our experiments with ion channels heterologously expressed in *Xenopus* oocytes CNTX did not significantly affect Nav currents, it is worth noting a small apparent decrease in the amplitude of Nav 1.6 channel current after the toxin application.

Our group previously reported on the membrane disturbing effect of JBU, a property that could underlie many of its biological activities. In nanomolar concentrations JBU forms ion channels in planar lipid bilayers consisting of mixtures of phosphatidylethanolamine (PE): phosphatidylcholine (PC): cholesterol (Ch) (Piovesan et al., 2014). Three types of conductance were observed, one main conductance displaying current rectification with conductance values of ~80 pS at positive voltages and ~44 pS at negative voltages, and two smaller non-rectifying conductances of ~30 and ~10 pS, respectively. The main channels formed by JBU were voltage-dependent, with a higher probability of opening at negative voltages, and strongly selective to cations (Piovesan et al., 2014). In another study (Micheletto et al., 2016), we investigated the interaction of JBU with liposomes with a lipid composition mimicking the human platelet membrane (34.1 % PC, 25.8 % Ch, 24.3 % PE, 7.7 % sphingomielin, 6.1 % phosphatidylserine and 2% phosphatidylinositol). Small angle X-ray scattering of multilamellar liposomes in the presence of JBU indicated a higher membrane rigidity due to the protein insertion into the lipid membrane(s). After 12 h of addition of JBU (500 nM), the membrane disorder caused by the protein's insertion changed the liposome organization mostly to a unilamellar state. These results shed some light on the biophysical aspects related to the property of urease(s) to interact with biological membranes (Micheletto et al., 2016).

A hypothesis that remains open for further investigations is if JBU can insert itself also into the much more complex biological membrane and affect its biophysical properties, in a dose dependent way. While the possibility of JBU forming itself cation selective pores in neuronal

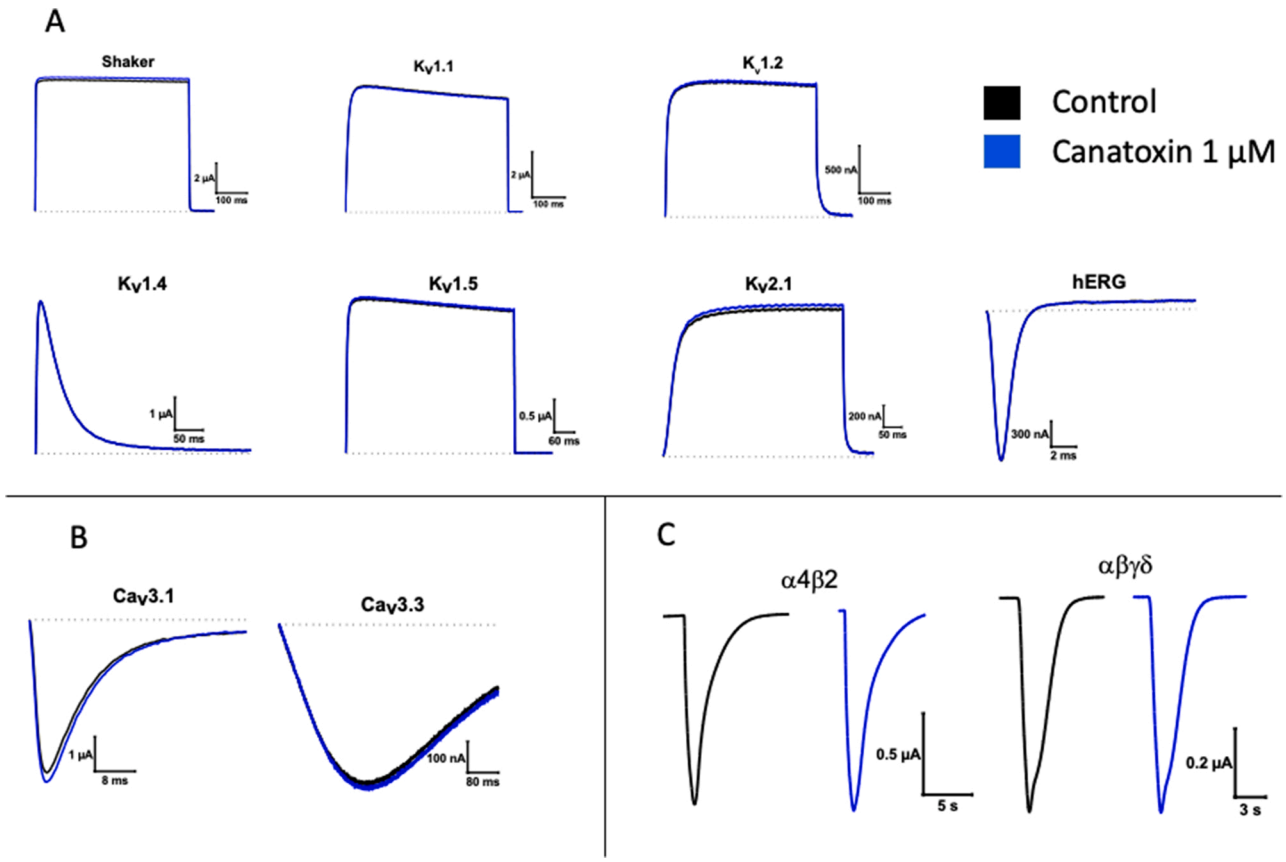

Fig. 7. Screening of Canatoxin effects on subtypes of voltage gated potassium and calcium channels, and in nicotinic receptors. *Xenopus* oocytes expressing the ion channels were perfused with 1 µM CNTX during 15 s at 3 mL.min^{-1}. Panel A) No significant changes in potassium current amplitude were observed in any of the tested potassium channels ($p < 0.05$, $n = 6$). Panel B) No significant changes in currents were observed in voltage gated T-type calcium channels ($p < 0.05$, $n = 6$) or Panel C) in acetylcholine nicotinic receptors ($p < 0.05$, $n = 6$). The acetylcholine pulses shown in black (controls) were applied manually in the perfusion system before canatoxin. Immediately after canatoxin perfusion, another acetylcholine pulse was given (blue current). These experiments were repeated at least with two different batches of CNTX.

membranes seems remote, the insertion of the protein into the biological membrane could disturb and affect the functions of nearby proteins such as ion channels and receptors.

3.9. [18]FDG microPET scans

[18]FDG uptake for the whole brain and subregions was calculated from microPET images of rats under the effect of 0.625 LD_{50} of CNTX (Fig. 8). A significant increase in glucose metabolism was seen in epileptogenic areas, such as hippocampus and thalamus.

The whole brain level of FDG uptake was ~27 % higher in treated rats than in controls, as expected for excitotoxic compounds. One striking feature in the microPET scans of treated animals was a higher metabolic activity in the areas responsible for breathing control such as pons, bulb and hypothalamus (Fig. 8A). Accordingly, CNTX-treated rats showed cyanosis, and bloody frothy sputum before seizures, consistent with hypoxia and respiratory distress. We have previously described that rats treated with convulsant doses of CNTX became cyanotic and experienced breathing distress (Ribeiro-DaSilva et al., 1989). These observations and the increased metabolic activity of brain areas responsible for breathing control, suggest a neurogenic pulmonary edema, a condition known to associate to epileptogenic activity (Finsterer, 2019; Sova et al., 2019).

Respiratory distress may not be the cause of urease-induced seizures, but it could be one of the key factors in the epileptogenesis associated to the toxin's effect.

4. Conclusion

There seems to be multiple mechanisms underlying the seizures induced by *C. ensiformis* ureases. The mode of action apparently is an indirect one as no effect was detected on several isolated ion channels and receptors. It is more likely that CNTX and JBU could be acting at a neuronal network level, thereby disturbing electroencephalographic rhythms and causing metabolic alterations in key areas related to epileptogenesis and to neurogenic pulmonary edema. In the context of neuroinflammation, modulation of lipoxygenase pathways in the CNS appears as interesting targets to focus aiming to unveil the action of these neurotoxins. The lack of LTP induction is more likely caused by a neuroprotection mechanism and/or release of lipoxygenase products than direct interaction of CNTX or JBU with receptors or ion channels. The previously reported lipoxygenase-mediated release of neurotransmitter now includes L-glutamate release, that could lead to excitotoxicity contributing to epileptogenesis. Accordingly, JBU increased calcium influx and neuronal firing rate in the hippocampus. [18]FDG microPET data indicated an increase in whole brain metabolism, and in areas related to epileptogenesis such as hippocampus and thalamus. A neurogenic pulmonary edema could be also implicated in the convulsant activity of canatoxin, as suggested by the higher [18]FDG uptake in areas responsible for breathing control. Altogether the data emphasize the complexity of the neurotoxic mechanism of action of *C. ensiformis* ureases. Considering that non-enzymatic properties are shared by ureases of different kingdoms, we hope that deepening the knowledge on the mechanism of neurotoxic action of *C. ensiformis* ureases would help to establish the relevance of these toxins in many infectious diseases caused

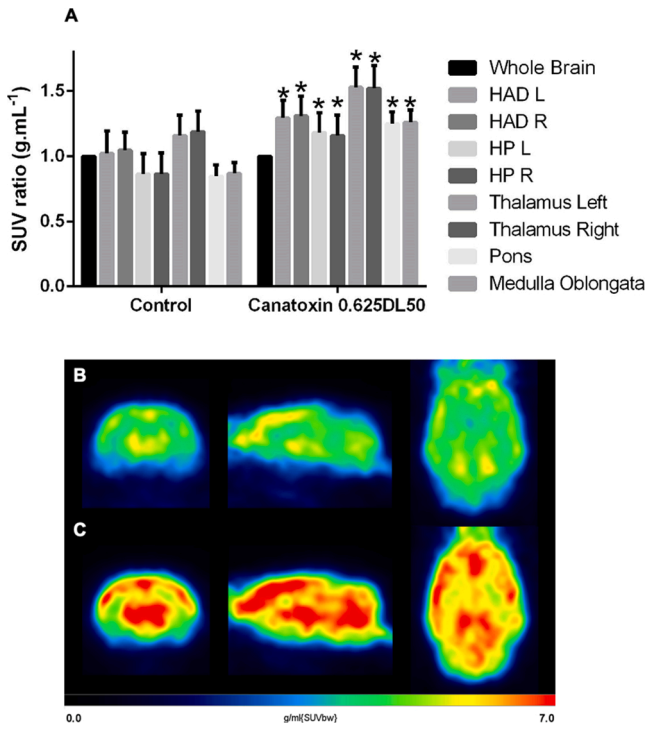

Fig. 8. ^{18}FDG microPositron Emission Tomography of CNTX-treated rats. Panel A $^{[18]}$FDG uptake in rat brain. The SUV ratio was normalized based on the whole brain FDG uptake. A significant increase in FDG metabolism on the measured brain areas was observed after 0.625DL$_{50}$ of canatoxin administration. HAD: Hippocampus Antero Dorsal, HP: Hippocampus posterior, L: Left, R: Right. Two way ANOVA for multiple comparisons, N = 9, $p < 0.05$. Panels B) and C) the images illustrate the ^{18}FDG uptake of rats brains during microPET-CT scans. Warmer colors indicate areas where the ^{18}FDG uptake values were higher, as colder colors indicate less ^{18}FDG uptake. Panel B shows representative brain images (three plans) of control animals; Panel C shows representative brain images (three plans) of rats treated with 0.625 LD$_{50}$ CNTX. Typical results.

by urease-producing microorganisms, in which the human central nervous system is affected.

CRediT authorship contribution statement

Carlos Gabriel Moreira Almeida: Investigation, Methodology, Formal analysis, Writing - original draft, Writing - review & editing. **Kiyo Costa-Higuchi:** Data curation, Formal analysis, Methodology, Software. **Angela Regina Piovesan:** Data curation, Formal analysis, Methodology. **Carlo Frederico Moro:** Methodology. **Gianina Teribele Venturin:** Methodology, Data curation, Software. **Samuel Greggio:** Methodology, Data curation, Software. **Zaquer Susana Costa-Ferro:** Methodology, Data curation. **Simone Denise Salamoni:** Methodology. **Steve Peigneur:** Methodology, Data curation, Formal analysis, Software, Supervision, Writing - review & editing. **Jan Tytgat:** Funding acquisition, Investigation, Project administration, Resources, Supervision, Writing - review & editing. **Maria Elena de Lima:** Resources, Supervision, Writing - review & editing. **Carolina Nunes da Silva:** Methodology, Data curation, Writing - review & editing. **Lúcia Vinadé:** Methodology, Supervision. **Edward G. Rowan:** Methodology, Resources, Supervision. **Jaderson Costa DaCosta:** Funding acquisition, Resources. **Chániston André Dal Belo:** Methodology, Data curation, Formal analysis, Investigation, Project administration, Supervision. **Celia Regina Carlini:** Conceptualization, Funding acquisition, Investigation, Project administration, Resources, Supervision, Validation, Visualization, Writing - original draft, Writing - review & editing.

Declaration of Competing Interest

The authors declare that they have no known competing financial interests or personal relationships that could have appeared to influence the work reported in this paper.

Acknowledgements

This work was supported by grants from the Brazilian agencies Coordenação de Aperfeiçoamento de Pessoal de Nível Superior (CAPES) –[finance code 001, and Edital 063/2010 Toxinologia [proj54/2011]; Conselho Nacional de Desenvolvimento Científico e Tecnológico (CNPq) – [Ed. Universal 2014 (No. 446052/2014-1) and Bolsa de Produtividade em Pesquisa (No. 306098/2014-8)], Fundação de Amparo à Pesquisa do Rio Grande do Sul (FAPERGS) [PPSUS 17/2551-0001451-0] and by Instituto Nacional de Ciência e Tecnologia (INCT) em Doenças Cerebrais e Excitotoxicidade [CNPq 465671/2014-4 and FAPERGS 17/2551-0000516-3]. C.G.M.A., K.C.H, C.F.M. and A.R.P. had fellowships from CAPES. J.C.C. and C.R.C. are Research Productivity grantees from CNPq. CADB is thankful to Dr. Trevor Bushell for receiving him in his laboratory at the University of Strathclyde, Scotland, and for teaching the calcium imaging methodology.

Appendix A. Supplementary data

Supplementary material related to this article can be found, in the online version, at doi:https://doi.org/10.1016/j.tox.2021.152737.

References

Akman, O., Demiralp, T., Ates, N., Onat, F.Y., 2010. Electroencephalographic differences between WAG/Rij and GAERS rat models of absence epilepsy. Epilepsy Res. 89, 185–193.
Alves, E.W., Ferreira, A.T., Ferreira, C.T., Carlini, C.R., 1992. Effects of canatoxin on the Ca(2+)-ATPase of sarcoplasmic reticulum membranes. Toxicon 30, 1411–1418.
Antonaccio, M.J., Taylor, D.G., 1977. Involvement of central GABA receptors in the regulation of blood pressure and heart rate of anesthetized cats. Eur. J. Pharmacol. 46, 283–287.
Bala, U., Tan, K.L., Ling, K.H., Cheah, P.S., 2014. Harvesting the maximum length of sciatic nerve from adult mice: a step-by-step approach. BMC Res. Notes 7, 714.
Baptista, P.P., Saur, L., Bagatini, P.B., Greggio, S., Venturin, G.T., Vaz, S.P., Ferreira Kdos, R., Junqueira, J.S., Lara, D.R., DaCosta, J.C., Jeckel, C.M., Mestriner, R.G., Xavier, L.L., 2015. Antidepressant effects of ketamine are not related to (1)(8)F-FDG metabolism or tyrosine hydroxylase immunoreactivity in the ventral tegmental area of wistar rats. Neurochem. Res. 40, 1153–1164.
Barja-Fidalgo, C., Guimaraes, J.A., Carlini, C.R., 1988. The secretory effect of canatoxin on rat brain synaptosomes involves a lipoxygenase-mediated pathway. Braz. J. Med. Biol. Res. 21, 549–552.
Barja-Fidalgo, C., Guimaraes, J.A., Carlini, C.R., 1991a. Canatoxin, a plant protein, induces insulin release from isolated pancreatic islets. Endocrinology 128, 675–679.
Barja-Fidalgo, C., Guimaraes, J.A., Carlini, C.R., 1991b. Lipoxygenase-mediated secretory effect of canatoxin the toxic protein from *Canavalia ensiformis* seeds. Toxicon 29, 453–459.
Bengtson, C.P., Kaiser, M., Obermayer, J., Bading, H., 2013. Calcium responses to synaptically activated bursts of action potentials and their synapse-independent replay in cultured networks of hippocampal neurons. Biochim. Biophys. Acta 1833, 1672–1679.
Bertram, E., 2007. The relevance of kindling for human epilepsy. Epilepsia 48 (Suppl 2), 65–74.
Bezanilla, F., 2006. The action potential: from voltage-gated conductances to molecular structures. Biol. Res. 39, 425–435.
Carlini, C.R., Guimaraes, J.A., 1981. Isolation and characterization of a toxic protein from *Canavalia ensiformis* (jack bean) seeds, distinct from concanavalin A. Toxicon 19, 667–675.
Carlini, C.R., Ligabue-Braun, R., 2016. Ureases as multifunctional toxic proteins: a review. Toxicon 110, 90–109.
Carlini, C.R., Gomes, C., Guimaraes, J.A., Markus, R.P., Sato, H., Trolin, G., 1984. Central nervous effects of the convulsant protein canatoxin. Acta Pharmacol. Toxicol. (Copenh) 54, 161–166.
Carlini, C.R., Guimaraes, J.A., Ribeiro, J.M., 1985. Platelet release reaction and aggregation induced by canatoxin, a convulsant protein: evidence for the involvement of the platelet lipoxygenase pathway. Br. J. Pharmacol. 84, 551–560.
Carrazoni, T., Nguyen, C., Maciel, L.F., Delgado-Cañedo, A., Stewart, B.A., Lange, A.B., Dal Belo, C.A., Carlini, C.R., Orchard, I., 2018. Jack bean urease modulates neurotransmitter release at insect neuromuscular junctions. Pest. Biochem. Phys. 146, 63–70.

Cordova, F.M., Rodrigues, A.L., Giacomelli, M.B., Oliveira, C.S., Posser, T., Dunkley, P.R., Leal, R.B., 2004. Lead stimulates ERK1/2 and p38MAPK phosphorylation in the hippocampus of immature rats. Brain Res. 998, 65–72.
Cornes, S.B., Griffin, E.A., Lownstein, D.H., 2014. Farmacologia da Neurotransmissão Eletrica Anormal no Sistema Nervoso Central. In: David, E.G., Armen, H.T., Ehrin, J. A., April, W.A. (Eds.), Principios de Farmacologia: A Base Fisiopatologica Da Farmacologia. Guanabara Koogan, Rio de Janeiro, pp. 227–241.
Costa-Ferro, Z.S., Vitola, A.S., Pedroso, M.F., Cunha, F.B., Xavier, L.L., Machado, D.C., Soares, M.B., Ribeiro-dos-Santos, R., DaCosta, J.C., 2010. Prevention of seizures and reorganization of hippocampal functions by transplantation of bone marrow cells in the acute phase of experimental epilepsy. Seizure 19, 84–92.
Dal Belo, C.A., Leite, G.B., Toyoma, M.H., Marangoni, S., Corrado, A.P., Fontana, M.D., Southan, A., Rowan, E.G., Hyslop, S., Rodrigues-Simioni, L., 2005. Pharmacological and structural characterization of a novel phospholipase A(2) from *Micrurus dumerilii* carinicauda venom. Toxicon 46, 736–750.
Dempster, J., 1993. Computer Analysis of Electrophysiological Signals. Academic Press, London.
Deshpande, S.B., 1998. Indian red scorpion (Mesobuthus tamulus concanesis, Pocock) venom prolongs repolarization time and refractoriness of the compound action potential of frog sciatic nerve in vitro through calcium dependent mechanism. Indian J. Exp. Biol. 36, 1108–1113.
Domingues, M.F., de Assis, D.R., Piovesan, A.R., Belo, C.A.D., da Costa, J.C., 2018. Peptide YY (3-36) modulates intracellular calcium through activation of the phosphatidylinositol pathway in hippocampal neurons. Neuropeptides 67, 1–8.
Dunkley, P.R., Jarvie, P.E., Robinson, P.J., 2008. A rapid Percoll gradient procedure for preparation of synaptosomes. Nat. Protoc. 3, 1718–1728.
Fan, D., Liu, S., Wang, Q., 2016. Stimulus-induced epileptic spike-wave discharges in thalamocortical model with disinhibition. Sci. Rep. 6, 37703.
Feinmark, S.J., Begum, R., Tsvetkov, E., Goussakov, I., Funk, C.D., Siegelbaum, S.A., Bolshakov, V.Y., 2003. 12-lipoxygenase metabolites of arachidonic acid mediate metabotropic glutamate receptor-dependent long-term depression at hippocampal CA3-CA1 synapses. J. Neurosci. 23, 11427–11435.
Finsterer, J., 2019. Neurological perspectives of neurogenic pulmonary edema. Eur. Neurol. 81, 94–102.
Follmer, C., Barcellos, G.B., Zingali, R.B., Machado, O.L.T., Alves, E.W., Barja-Fidalgo, C., Guimaraes, J.A., Carlini, C.R., 2001. Canatoxin, a toxic protein from jack beans (*Canavalia ensiformis*), is a variant form of urease (EC 3.5.1.5): biological effects of urease independent of its ureolytic activity. Biochem. J. 360, 217–224.
Follmer, C., Pereira, F.V., Da Silveira, N.P., Carlini, C.R., 2004a. Jack bean urease (EC 3.5.1.5) aggregation monitored by dynamic and static light scattering. Biophys. Chem. 111, 79–87.
Follmer, C., Real-Guerra, R., Wasserman, G.E., Olivera-Severo, D., Carlini, C.R., 2004b. Jackbean, soybean and *Bacillus pasteurii* ureases - Biological effects unrelated to ureolytic activity. Eur. J. Biochem. 271, 1357–1363.
Ghazaleh, F.A., Francischetti, I.M., Gombarovits, M.E., Carlini, C.R., 1997. Stimulation of calcium influx and platelet activation by canatoxin: methoxyverapamil inhibition and downregulation by cGMP. Arch. Biochem. Biophys. 339, 362–367.
Grassi-Kassisse, D.M., Ribeiro-DaSilva, G., 1992. Canatoxin triggers histamine secretion from rat peritoneal mast cells. Agents Actions 37, 204–209.
Hedou, G.F., Koshibu, K., Farinelli, M., Kilic, E., Gee, C.E., Kilic, U., Baumgartel, K., Hermann, D.M., Mansuy, I.M., 2008. Protein phosphatase 1-dependent bidirectional synaptic plasticity controls ischemic recovery in the adult brain. J. Neurosci. 28, 154–162.
Henshall, D.C., 2007. Apoptosis signalling pathways in seizure-induced neuronal death and epilepsy. Biochem. Soc. Trans. 35, 421–423.
Iftinca, M.C., 2011. Neuronal T-type calcium channels: what's new? Iftinca: T-type channel regulation. J. Med. Life 4, 126–138.
Jan, A.T., 2017. Outer membrane vesicles (OMVs) of gram-negative Bacteria: a perspective update. Front. Microbiol. 8, 1053.
Jeffery, C.J., 1999. Moonlighting proteins. Trends Biochem. Sci. 24, 8–11.
Kappaun, K., Piovesan, A.R., Carlini, C.R., Ligabue-Braun, R., 2018. Ureases: historical aspects, catalytic, and non-catalytic properties - a review. J. Adv. Res. 13, 3–17.
Kawa, K., 1990. Voltage-gated calcium and potassium currents in megakaryocytes dissociated from guinea-pig bone marrow. J. Physiol. 431, 187–206.
Kovacs, Z., Kekesi, K.A., Juhasz, G., Dobolyi, A., 2015. Modulatory effects of inosine, guanosine and uridine on lipopolysaccharide-evoked increase in spike-wave discharge activity in Wistar Albino Glaxo/Rijswijk rats. Brain Res. Bull. 118, 46–57.
Kullmann, D.M., Asztely, F., Walker, M.C., 2000. The role of mammalian ionotropic receptors in synaptic plasticity: LTP, LTD and epilepsy. Cell. Mol. Life Sci. 57, 1551–1561.
Lamothe, S.M., Zhang, S., 2016. Ubiquitination of Ion Channels and Transporters. Progress in Molecular Biology and Translational Science. Elsevier Inc., pp. 161–223
Liman, E.R., Tytgat, J., Hess, P., 1992. Subunit stoichiometry of a mammalian K+ channel determined by construction of multimeric cDNAs. Neuron 9, 861–871.
Liu, Y., Peterson, D.A., Kimura, H., Schubert, D., 1997. Mechanism of cellular 3-(4,5-dimethylthiazol-2-yl)-2,5-diphenyltetrazolium bromide (MTT) reduction. J. Neurochem. 69, 581–593.
Loiseau, P., 1992. Human absence epilepsies. J. Neural Transm. Suppl. 35, 1–6.
Lomeo Rda, S., Goncalves, A.P., da Silva, C.N., de Paula, A.T., Costa Santos, D.O., Fortes-Dias, C.L., Gomes, D.A., de Lima, M.E., 2014. Crotoxin from *Crotalus durissus terrificus* snake venom induces the release of glutamate from cerebrocortical synaptosomes via N and P/Q calcium channels. Toxicon 85, 5–16.
Mahaut-Smith, M.P., 2012. The unique contribution of ion channels to platelet and megakaryocyte function. J. Thromb. Haemost. 10, 1722–1732.
Mantegazza, M., Gambardella, A., Rusconi, R., Schiavon, E., Annesi, F., Cassulini, R.R., Labate, A., Carrideo, S., Chifari, R., Canevini, M.P., Canger, R., Franceschetti, S., Annesi, G., Wanke, E., Quattrone, A., 2005. Identification of an Nav1.1 sodium channel (SCN1A) loss-of-function mutation associated with familial simple febrile seizures. Proc. Natl. Acad. Sci. U. S. A. 102, 18177–18182.
Mantegazza, M., Curia, G., Biagini, G., Ragsdale, D.S., Avoli, M., 2010. Voltage-gated sodium channels as therapeutic targets in epilepsy and other neurological disorders. Lancet Neurol. 9, 413–424.
McCormick, D.A., Contreras, D., 2001. On the cellular and network bases of epileptic seizures. Annu. Rev. Physiol. 63, 815–846.
Meldrum, B.S., 1994. The role of glutamate in epilepsy and other CNS disorders. Neurology 44, S14–23.
Micheletto, Y.M.S., Moro, C.F., Lopes, F.C., Ligabue-Braun, R., Martinelli, A.H.S., Marques, C.M., Schroder, A.P., Carlini, C.R., Silveira, N.P., 2016. Interaction of jack bean (*Canavalia ensiformis*) urease and a derived peptide with lipid vesicles. Colloids Surf. B 145, 576–585.
Milligan, G., 2003. Constitutive activity and inverse agonists of G protein-coupled receptors: a current perspective. Mol. Pharmacol. 64, 1271–1276.
Mortimer, J.T., Badra, N., 2003. Compound Action Potentials: Problems When Testing for Block.
Normandin, M., Gagne, J., Bernard, J., Elie, R., Miceli, D., Baudry, M., Massicotte, G., 1996. Involvement of the 12-lipoxygenase pathway of arachidonic acid metabolism in homosynaptic long-term depression of the rat hippocampus. Brain Res. 730, 40–46.
Onizuka, S., Kasaba, T., Hamakawa, T., Takasaki, M., 2005. Lidocaine excites both pre- and postsynaptic neurons of reconstructed respiratory pattern generator in Lymnaea stagnalis. Anesth. Analg. 100, 175–182.
Papale, L.A., Beyer, B., Jones, J.M., Sharkey, L.M., Tufik, S., Epstein, M., Letts, V.A., Meisler, M.H., Frankel, W.N., Escayg, A., 2009. Heterozygous mutations of the voltage-gated sodium channel SCN8A are associated with spike-wave discharges and absence epilepsy in mice. Hum. Mol. Genet. 18, 1633–1641.
Paxinos, G., Watson, C., 2007. The Rat Brain in Stereotaxic Coordinates. Academic Press.
Peigneur, S., Devi, P., Seldeslachts, A., Ravichandran, S., Quinton, L., Tytgat, J., 2019. Structure-Function Elucidation of a New alpha-Conotoxin, MilIA, from*Conus milneedwardsi*. Mar. Drugs 17.
Persson, B., Henning, M., 1980. Effect of GABA analogues on blood pressure and central GABA metabolism in the rat. Acta Pharmacol. Toxicol. (Copenh) 47, 135–143.
Piovesan, A.R., Martinelli, A.H.S., Ligabue-Braun, R., Schwartz, J.L., Carlini, C.R., 2014. *Canavalia ensiformis* urease, Jaburetox and derived peptides form ion channels in planar lipid bilayers. Arch. Biochem. Biophys. 547, 6–17.
Rang, H., Dale, M.M., Ritter, J.M., Flower, R.J., Henderson, G., 2016. Farmacologia. Elsevier Editora Ltda Brasil, São Paulo.
Ribeirodasilva, G., Prado, J.F., 1993. Increased insulin circulating levels induced by canatoxin in rats. Toxicon 31, 1131–1136.
Ribeiro-DaSilva, G., Pires Barbosa, R., Prado, J.F., Carlini, C.R., 1989. Convulsions induced by canatoxin in rats are probably a consequence of hypoxia. Braz. J. Med. Biol. Res. 22, 877–880.
Riddles, P.W., Whan, V., Blakeley, R.L., Zerner, B., 1991. Cloning and sequencing of a jack bean urease-encoding cDNA. Gene 108, 265–267.
Saur, L., Neves, L.T., Greggio, S., Venturin, G.T., Jeckel, C.M.M., Costa Da Costa, J., Bertoldi, K., Schallenberger, B., Siqueira, I.R., Mestriner, R.G., Xavier, L.L., 2017. Ketamine promotes increased freezing behavior in rats with experimental PTSD without changing brain glucose metabolism or BDNF. Neurosci. Lett. 658, 6–11.
Skowronska, M., Albrecht, J., 2012. Alterations of blood brain barrier function in hyperammonemia: an overview. Neurotox. Res. 21, 236–244.
Snead 3rd, O.C., 1995. Basic mechanisms of generalized absence seizures. Ann. Neurol. 37, 146–157.
Soderlund, D.M., Tan, J., He, B., 2017. Functional reconstitution of rat Nav1.6 sodium channels in vitro for studies of pyrethroid action. Neurotoxicology 60, 142–149.
Sova, M., Franc, D., Ctvrtlik, F., Jakubec, P., Ghazal Asswad, A., Kolek, V., 2019. Neurogenic pulmonary oedema as a rare complication of epileptic seizures. Adv. Respir. Med. 87, 298–300.
Staniscuaski, F., Brugge, V.T., Carlini, C.R., Orchard, I., 2009. In vitro effect of *Canavalia ensiformis* urease and the derived peptide Jaburetox-2Ec on *Rhodnius prolixus* Malpighian tubules. J. Insect Physiol. 55, 255–263.
Treiman, D.M., 2001. GABAergic mechanisms in epilepsy. Epilepsia 42 (Suppl 3), 8–12.
Vinade, L., Rodnight, R., 1996. The dephosphorylation of glial fibrillary acidic protein (GFAP) in the immature rat hippocampus is catalyzed mainly by a type 1 protein phosphatase. Brain Res. 732, 195–200.
Weber, M., Jones, M.J., Ulrich, J., 2008. Optimisation of isolation, and purification of the jack bean enzyme urease by extraction and subsequent crystallization. Food Bioprod. Process. 86, 43–52.
Whitt, J.P., McNally, B.A., Meredith, A.L., 2018. Differential contribution of Ca(2+) sources to day and night BK current activation in the circadian clock. J. Gen. Physiol. 150, 259–275.
Wilson, M.J., Yoshikami, D., Azam, L., Gajewiak, J., Olivera, B.M., Bulaj, G., Zhang, M. M., 2011. mu-Conotoxins that differentially block sodium channels NaV1.1 through 1.8 identify those responsible for action potentials in sciatic nerve. Proc. Natl. Acad. Sci. U. S. A. 108, 10302–10307.
Yu, F.H., Catterall, W.A., 2004. The VGL-chanome: a protein superfamily specialized for electrical signaling and ionic homeostasis. Sci. STKE 2004 re15.
Zanirati, G., Azevedo, P.N., Venturin, G.T., Greggio, S., Alcara, A.M., Zimmer, E.R., Feltes, P.K., DaCosta, J.C., 2018. Depression comorbidity in epileptic rats is related to brain glucose hypometabolism and hypersynchronicity in the metabolic network architecture. Epilepsia 59, 923–934.
Zhang, C.H., Sha, Z., Mundahl, J., Liu, S., Lu, Y., Henry, T.R., He, B., 2015. Thalamocortical relationship in epileptic patients with generalized spike and wave discharges–A multimodal neuroimaging study. Neuroimage Clin. 9, 117–127.

Zhang, S., Zhu, Y., Cheng, J., Tao, J., 2019. Ion Channels in Epilepsy: Blasting Fuse for Neuronal Hyperexcitability. Epilepsy - Advances in Diagnosis and Therapy. IntechOpen.
Zhu, Y., Zhang, S., Feng, Y., Xiao, Q., Cheng, J., Tao, J., 2018. The yin and Yang of BK channels in epilepsy. CNS Neurol. Disord. Drug Targets 17, 272–279.
Zschauer, A., van Breemen, C., Buhler, F.R., Nelson, M.T., 1988. Calcium channels in thrombin-activated human platelet membrane. Nature 334, 703–705.
Zsurka, G., Kunz, W.S., 2015. Mitochondrial dysfunction and seizures: the neuronal energy crisis. Lancet Neurol. 14, 956–966.